



**EFFECTS OF MAGNETIC INDUCEMENT ON
Cu-Zn/CeO₂-DOPED Al₂O₃ CATALYST FOR
METHANOL STEAM REFORMING**

BY

MRS. DILPIUM SAMARASINGHE

**A THESIS SUBMITTED IN PARTIAL FULFILLMENT OF THE
REQUIREMENTS FOR THE DEGREE OF MASTER OF
SCIENCE (ENGINEERING AND TECHNOLOGY)
SIRINDHORN INTERNATIONAL INSTITUTE OF TECHNOLOGY
THAMMASAT UNIVERSITY
ACADEMIC YEAR 2019
COPYRIGHT OF THAMMASAT UNIVERSITY**

**EFFECTS OF MAGNETIC INDUCEMENT ON
Cu-Zn/CeO₂-DOPED Al₂O₃ CATALYST FOR
METHANOL STEAM REFORMING**

BY

MRS. DILPIUM SAMARASINGHE

**A THESIS SUBMITTED IN PARTIAL FULFILLMENT OF THE
REQUIREMENTS FOR THE DEGREE OF MASTER
OF SCIENCE (ENGINEERING AND TECHNOLOGY)
SIRINDHORN INTERNATIONAL INSTITUTE OF TECHNOLOGY
THAMMASAT UNIVERSITY
ACADEMIC YEAR 2019
COPYRIGHT OF THAMMASAT UNIVERSITY**

THAMMASAT UNIVERSITY
SIRINDHORN INTERNATIONAL INSTITUTE OF TECHNOLOGY

THESIS

BY

MRS. THALPAVILA KANKANAMGE SHYAMALA DILPIUM
SAMARASINGHE

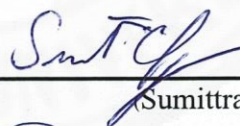
ENTITLED

EFFECTS OF MAGNETIC INDUCEMENT ON Cu-Zn/CeO₂ DOPED Al₂O₃
CATALYST FOR METHANOL STEAM REFORMING

was approved as partial fulfillment of the requirements for
the degree of Master of Science (Engineering and Technology)

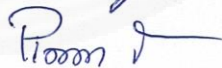
on July 31, 2020

Chairperson



(Sumittra Charojrochkul, Ph.D.)

Member and Advisor



(Associate Professor Pisanu Toochinda, Ph.D.)

Member



(Associate Professor Luckhana Lawtrakul, Dr.rer.nat.)

Director



(Professor Pruettha Nanakorn, D.Eng.)

Thesis Title	EFFECTS OF MAGNETIC INDUCEMENT ON Cu-Zn/CeO ₂ -DOPED Al ₂ O ₃ CATALYST FOR METHANOL STEAM REFORMING
Author	Mrs. Dilpium Samarasinghe
Degree	Master of Science (Engineering and Technology)
Faculty/University	Sirindhorn International Institute of Technology/ Thammasat University
Thesis Advisor	Associate Professor Oisanu Toochinda, Ph.D.
Academic Years	2019

ABSTRACT

The active Cu-Zn catalyst can be developed for H₂ production from methanol steam reforming (MSR) at low temperatures. Here the Cu-Zn catalyst is developed through support modification and enhancing dispersion of active metals on the catalyst support. The conventional γ -Al₂O₃ support is modified by partial doping of Ce into Al₂O₃ framework. Then magnetic inducement is applied during the sol-gel preparation of CeO₂-doped Al₂O₃ support. A good Cu-Zn catalyst for MSR requires Cu and Zn cluster to be deposited together to provide Cu⁺ which is the perfect active site for MSR. The magnetic inducement is introduced during sol-gel preparation of catalyst by applying different magnetic pole arrangements (N-N, N-S, and without magnetic inducement) to investigate their ability to disperse and control Cu and Zn deposition. The catalytic activity for H₂ productions are evaluated at the temperatures of 200 °C–300 °C in continuous mode. The catalysts and supports are analyzed through SEM-EDS, XRD, XPS, and BET surface area to determine the Cu-Zn dispersion over supports and Ce dispersion on the CeO₂-doped Al₂O₃ supports. The results show that the combination of partial doping of Ce into Al₂O₃ framework and magnetic inducement during support preparation process improves the hydrogen production rate. And also the combined application of magnetic pole arrangement during the sol-gel preparation of CeO₂-doped Al₂O₃ support and Cu-Zn metal loading on the support, and

enhances the catalytic activity of prepared catalysts compared to the catalysts prepared under separate application of magnetic inducements. Further, the concentration profiles of Cu^{2+} and Zn^{2+} ions on $\alpha\text{-Al}_2\text{O}_3$ support show that irrespective of the magnetic pole arrangement, magnetic inducement is capable of providing an external driving force for the ions to be dispersed homogeneously on any support.

Keywords: Cu-Zn catalyst, Support modification, CeO_2 -doped Al_2O_3 support, Magnetic inducement, Methanol steam reforming



ACKNOWLEDGEMENTS

I will not be able to complete my master degree without the care, support and guidance from a group of special people. First, I would like to express my sincere gratitude to my advisor, Associate Professor Dr. Pisanu Toochinda for his kind & generous support, extensive guidance and caring attention throughout my study. Moreover, I would like to thank the thesis committee members, Associate Professor Dr. Luckhana Lawtrakul and Dr. Sumittra Charojrochkul for their contributions and comments to improve the quality of this work.

I would like to thank my research and laboratory seniors, Mr. Pumiwat Vacharapong, Ms. Sirinta Arayawate, and Ms. Sasimas Katanyutanon for their kind helps, knowledge and supports during my academic works and laboratory experiments. And also I would like to thank the BCET laboratory staff Ms. Atitaya Kuwalairat and Mr. Prasitchai Chaiamarit for their kind guidance during my laboratory experiments. And I would also like to thank Mr. Mahinsasa Rathnayake, who helped me personally during early days of my master degree. In addition, I would like to thank the graduate colleagues and the officials in the school of Bio-chemical Engineering and Technology, including the secretary of school of BCET Ms. Suwanna Punyadee and Sirindhorn International Institute of Technology for their helps in various way during my study.

I would like to acknowledge Thammasat University Grant for the support on my research work during my study. I am so much grateful to the Excellent Foreign Student (EFS) scholarship program of Sirindhorn International Institute of Technology, Thammasat University that provided me a full scholarship opportunity with living allowance for my master study.

Lastly I would like to thank my family my father Mr. Somavijaya Samarasinghe, my mother, Mrs. Priyangani Wanasinghe, and my husband Mr. Rumesh Wishwa for supporting me physically and mentally.

Mrs. Dilpium Samarasinghe

TABLE OF CONTENTS

	Page
ABSTRACT	(1)
ACKNOWLEDGEMENTS	(3)
LIST OF TABLES	(8)
LIST OF FIGURES	(9)
LIST OF SYMBOLS/ABBREVIATIONS	(10)
CHAPTER 1 INTRODUCTION	1
1.1 Statement	1
1.2 Objective	4
1.3 Scope of the study	4
1.3.1 Support modification	4
1.3.2 Enhancement of active Cu-Zn metal dispersion on the support	5
CHAPTER 2 REVIEW OF LITERATURE	7
2.1 Hydrogen production	7
2.2 Hydrogen production from methanol	10
2.3 Methanol steam reforming reaction	12
2.4 Catalysts for methanol steam reforming reaction	13
2.5 Supports for Cu based catalysts	18
2.5.1 Structure of Al ₂ O ₃	18
2.5.2 Properties of CeO ₂	20
2.5.2.1 Interactions with hydrogen	22
2.5.2.2 Interactions with carbon monoxide	26

	(5)
2.5.2.3 Interactions with hydrocarbons	26
2.5.3 CeO ₂ -doped γ -Al ₂ O ₃ support	28
2.5.3.1 Viscosity test	28
2.5.3.2 Thermogravimetric analysis (TGA)	28
2.5.3.3 Hydrogen temperature programmed reduction (H ₂ -TPR)	29
2.6 Oxygen vacancy	30
2.7 Catalyst preparation methods	31
2.8 Effect of magnetic field towards ions	31
CHAPTER 3 METHODOLOGY	35
3.1 Chemicals and materials	35
3.2 Catalyst preparation	35
3.2.1 Preparation of CeO ₂ -doped γ -Al ₂ O ₃ support	35
3.2.2 Preparation of Cu-Zn/CeO ₂ -doped Al ₂ O ₃ catalyst	37
3.2.3 Preparation of Cu-Zn/ α -Al ₂ O ₃ catalyst	37
3.2.3.1 Microwave acid digestion method for Cu/ α -Al ₂ O ₃ catalyst	38
3.2.3.2 Microwave acid digestion method for Zn/ α -Al ₂ O ₃ catalyst	40
3.2.3.3 Microwave acid digestion method for Cu-Zn/ α -Al ₂ O ₃ catalyst	40
3.3 Methanol steam reforming reaction	41
3.3.1 Catalytic activity test	41
3.4 Characterization	41
3.4.1 Support characterization	41
3.4.1.1 BET analyzer	41
3.4.1.2 X-ray diffraction (XRD)	42
3.4.1.3 Scanning electron microscopy with energy dispersive spectroscopy (SEM-EDS)	43
3.4.1.4 X-ray photoelectron spectroscopy (XPS)	44
3.4.2 Catalyst characterization	44
3.4.2.1 Atomic absorption spectroscopy (AAS)	44

	(6)
CHAPTER 4 RESULTS AND DISCUSSION	45
4.1 Effect of magnetic inducement on preparation of 5mol% CeO ₂ -doped Al ₂ O ₃ support	45
4.1.1 Hydrogen production rates obtained through MSR	45
4.1.2 Doping of Ce into Al ₂ O ₃ framework with and without magnetic inducement	46
4.1.3 Dispersion of Ce in the Al ₂ O ₃ framework with and without magnetic inducement	49
4.2. Effect of magnetic inducement on motion of Cu ²⁺ and Zn ²⁺ ions in sol-gel media	54
4.2.1 Diffusion of Cu ²⁺ ions on α-Al ₂ O ₃ support under magnetic inducement	55
4.2.2 Diffusion of Zn ²⁺ ions on α-Al ₂ O ₃ support under magnetic inducement	56
4.2.3 Combined diffusion of Cu ²⁺ and Zn ²⁺ ions on α-Al ₂ O ₃ support under magnetic inducement	57
4.3 Effect of magnetic inducement on deposition and distribution of Cu and Zn active metals on support	58
4.3.1 Hydrogen production yield through MSR	58
4.4 Effect of magnetic inducement during both support preparations and active metal loading on the support	59
4.4.1 Hydrogen production yield through MSR	60
CHAPTER 5 CONCLUSIONS	61
REFERENCES	63
APPENDICES	73
APPENDIX A	74
APPENDIX B	77
BIOGRAPHY	79

LIST OF TABLES

Tables	Page
2.1 Overview of hydrogen production methods by primary energy and material source	9
2.2 Reaction conditions and hydrogen yield for methanol steam reforming reaction (MSR) by various Cu-based catalysts	17
3.1 List of chemicals used in experiments	36
4.1 H ₂ production rate over 5wt% Cu-Zn catalysts (no magnet) on 5mol% CeO ₂ -doped Al ₂ O ₃ supports prepared with and without magnetic inducement	46
4.2 Lattice parameters derived from XRD graph	47
4.3 BET surface area data	48
4.4 Ce distribution in CeO ₂ -doped Al ₂ O ₃ with and without magnetic inducement	50
4.5 Peak energy of Al 2p and Ce 3d XPS spectrograms (Vacharapong et al., 2019)	53
4.6 H ₂ production rate over 5wt% Cu-Zn/ In-house γ -Al ₂ O ₃ catalysts prepared with and without magnetic inducement	58
4.7 H ₂ production rate of 5wt% Cu-Zn catalyst prepared with and without magnetic inducement over 5mol% CeO ₂ -doped Al ₂ O ₃ (no magnet) support	60
4.8 H ₂ production rate of 5wt% Cu-Zn catalyst prepared with and without magnetic inducement over 5mol% CeO ₂ -doped Al ₂ O ₃ (N-N) support	61
4.9 H ₂ production rate of 5wt% Cu-Zn catalyst prepared with and without magnetic inducement over 5mol% CeO ₂ -doped Al ₂ O ₃ (N-S) support	61
A.1 Molecular weight of related metals or compounds in support preparation	74
A.2 Calculated amount of metals used in support preparation	74
A.3 Calculated amount of compounds used in support preparation	75
A.4 Molecular weight of related metals or compounds in catalyst preparation	75
A.5 Calculated amount of compounds used in catalyst preparation	76

LIST OF FIGURES

Figures	Page
1.1 Graphical summary of support modification	5
1.2 Graphical summary of Cu-Zn metal dispersion on γ -Al ₂ O ₃ support	5
1.3 Graphical summary of Cu-Zn metal dispersion on CeO ₂ -doped Al ₂ O ₃ support	6
2.1 Experimental cubic γ -Al ₂ O ₃ spinel-type unit cell (Trueba & Trasatti, 2005)	20
2.2 The fcc unit cell of CeO ₂ with the fluorite structure (Trovarelli, 1996)	22
2.3 TPR of CeO ₂ samples. (A) CeO ₂ BET surface area 1 m ² /g (B) CeO ₂ BET surface area 10 m ² /g (Hickey et al., 2001)	23
2.4 Pathway proposed for CeO ₂ surface reduction (El Fallah et al., 1994)	24
2.5 Extent of CeO ₂ reduction vs. temperature for CeO ₂ , CeO ₂ (28.4%)/SiO ₂ , and CeO ₂ (1.6%)/SiO ₂ as determined from TPR analysis (De Leitenburg, Trovarelli, & Kašpar, 1997)	26
2.6 Methane adsorbed on two different sites of ceria (Trovarelli, 1996)	28
2.7 Adsorption of HC on acid-base sites of CeO ₂ (Trovarelli, 1996)	29
2.8 A charged particle having a velocity vector that has a component parallel to a uniform magnetic field moves in a helical path (Halliday et al., 2013)	34
3.1 Magnetic device component and set up	37
3.2 Schematic of magnetic device for sol-gel support preparation	38
3.3 Geometrical image of alpha alumina powder plate	39
3.4 Schematic of lab scale methanol steam reforming process	41
3.5 BET analyzer (N ₂ physical adsorption instrument)	42
3.6 X - ray diffraction instrument	43
3.7 Scanning Electron Microscopy with Energy Dispersive Spectroscopy	44
4.1 SEM images and scanning points of CeO ₂ -doped Al ₂ O ₃ supports with and without magnetic inducement	49
4.2 Schematics of Ce ³⁺ and Al ³⁺ movement under (a) no magnetic inducement (b) magnetic field from opposite magnetic field arrangement (N-S) and (c) same pole magnetic arrangement (N-N) (Vacharapong et al., 2019)	51
4.3 Al 2p XPS spectrograms of Al ₂ O ₃ and CeO ₂ -doped Al ₂ O ₃ prepared with and	

	(9)
without magnetic inducements (Vacharapong et al., 2019)	52
4.4 Ce 3d XPS spectrograms of CeO ₂ -doped Al ₂ O ₃ prepared with and without Magnetic inducement (Vacharapong et al., 2019)	53
4.5 Geometrical dimension of α -Al ₂ O ₃ powder plate	54
4.6 Concentration profile of diffusion of Cu ²⁺ ions on α -Al ₂ O ₃ support	55
4.7 Concentration profile of diffusion of Zn ²⁺ ions on α -Al ₂ O ₃ support	56
4.8 Concentration profile of diffusion of Cu ²⁺ and Zn ²⁺ ions on α -Al ₂ O ₃ support	57
B.1 Diagram for temperature-programmed reduction (TPR) and temperature- programmed oxidation (TPO) explanation (BEL JAPAN INC., 2012)	77



LIST OF SYMBOLS/ABBREVIATIONS

Symbols/Abbreviations	Terms
SIIT	Sirindhorn International Institute of Technology
TU	Thammasat University
*	Vacant active site
σ_m	Cross-sectional area of one metal atom (nm^2)
ΔH	Enthalpy, Heat of reaction
$^{\circ}\text{C}$	Degree Celsius
\AA	Angstrom
A	Pre-exponential factor (Arrhenius equation), Amp (current)
a.u.	Arbitrary unit
Al	Aluminium
$\text{Al}(\text{NO}_3)_3 \cdot 9\text{H}_2\text{O}$	Aluminum nitrate nonahydrate
Al_2O_3	Aluminum Oxide (Alumina)
Al^{3+}	Aluminium ion
Ar	Argon
atm	Atmosphere (pressure unit)
B	Magnetic field
BD	Butadiene
BET	Brunauer-Emmett-Teller, Technique
C	Carbon
Ce	Cerium
$\text{Ce}(\text{NO}_3)_3 \cdot 6\text{H}_2\text{O}$	Cerium (III) nitrate hexahydrate
Ce^{3+}	Cerium(III) ion
Ce^{4+}	Cerium(IV) ion
CeO_2	Cerium(IV) oxide (Cerium)

CH ₄	Methane
CHN	Carbon-Hydrogen-Nitrogen
cm ³	Cubic centimeter (volume)
CNTs	Carbon nanotubes
CO	Carbon monoxide
C-O	Carbon-oxygen bond
Co	Cobalt
CO ₂	Carbon dioxide
CP	Co-precipitation method
Cu	Copper
C _x H _y	Hydrocarbon species
DI	Deionized
e ⁻	Electron
e ⁺	Positron
E _a	Activation energy
E _{ads}	Adsorption energy
EFS	Excellent Foreign Student
eV	Electron volt (energy unit)
FB	Magnetic force
Fe	Iron
Fe ₂ O ₄	Iron(II) oxide
g	gram (weight)
GC	Gas Chromatography
GCMS	Gas chromatography coupled with mass spectrometer
h	Hour (time)
H ₂	Hydrogen
H ₂ O	Water
He	Helium
ID	Inner diameter
J	Joule

K	Kelvin (Temperature)
k	kilo (10 ³)
l, L	Liter (volume)
m	Sample weight (g)
m	Meter (length)
M	Molar (concentration)
m/z	mass-to-charge ratio
m ²	Square meter (area)
Mg	Magnesium
MgAl ₂ O ₄	Magnesium Aluminum spinel
MgO	Magnesium Oxide (Magnesia)
min	Minute (time)
mol%	Mole percent
MW	Atomic weight of metal (g mol ⁻¹)
N	Nitrogen atom
N ₂	Nitrogen gas
N-N	North-North
N-S	North-South
O	Oxygen atom
O ₂	Oxygen gas
OSC	Oxygen storage capacity
p	weight percentage of supported metal content (wt%)
Pd	Palladium
pH	-log[H ⁺]
POX	Partial oxidation
ppm	Part per million
Pt	Platinum
PV	Photovoltaic
Q	Charge of the particle
Rh	Rhodium
Ru	Ruthenium

SA	Surfactant-assisted method
sec	Second (time)
SEM-EDS	Scanning Electron Microscopy with Energy Dispersive Spectroscopy
SG	Sol-gel method
SiO ₂	Silicon dioxide, Silica
SR	Steam reforming
T	Temperature
TEM	Transmission Electron Microscopy
TiO ₂	Titanium dioxide Titanium(IV) oxide (Titania)
TPD	Temperature-programmed desorption
TPRx	Temperature-programmed reaction
v	Velocity of the moving particle
V	Volt
V _{chem}	Amount of adsorption (cm ³)
vol%	Volume percent
WGSR	Water-gas-shift reaction
wt%	Weight percent
XRD	X-ray Diffraction
Zn	Zinc
Zn ²⁺	Zinc ion
Zn(NO ₃) ₂ .6H ₂ O	Zinc nitrate
ZnO	Zinc oxide
Zr	Zirconium
γ	gamma
μ	Micro
ρ	Density of metal (g/cm ³)

CHAPTER 1

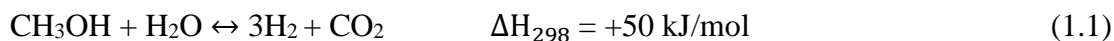
INTRODUCTION

1.1 Statement

Since there is an immense demand for fossil fuels, global energy consumption is subjected to a rapid increment. The limited amount of fossil fuel has become a major concern of energy inadequacy. For instance, greenhouse gases produced mainly from the burning of automobile fuel causes impacts on world climate and ecology. Thus these environmental issues have dragged global attention during recent years, where it is crucial to carry out researches and develop new pollution-free energy sources. Thus the production of electrical energy with fuel cells is a very eco-friendly technology that has been investigated often. Although this technique has very low or no gas emissions, a large amount of energy is required to generate a reasonable amount of hydrogen (H₂) to form hydrogen fuel cells, making this process expensive. Many methods such as steam reforming, partial oxidation, plasma reforming can be used to produce hydrogen (Chiu, Chiu, Hsieh, Jang, & Syu, 2017).

One of the most well-known methods for hydrogen production is the steam reforming of hydrocarbons because of its efficiency and economic cost. Hydrocarbons that can be used in steam reforming include methanol, ethanol, and natural gases. In comparison to other fuel sources, methanol is much convenient based on several unique characteristics. Methanol stays in the liquid state at room temperature and has a relatively high H:C ratio of 4:1 which may provide more hydrogen yield. And also since it has no strong C-C bond in its chemical structure, it lowers the risk of requiring high temperature for the generation of hydrogen and hinders the formation of coke during the reaction (Oguchi, Nishiguchi, Matsumoto, & Kanai, 2005).

Several chemical reactions can be implemented for the conversion of methanol to hydrogen energy, among them steam reforming of methanol provides the highest amount of hydrogen yield (Azenha, Mateos-Pedrero, Queirós, Concepción, & Mendes, 2017).



Although the production of hydrogen is the prominent goal of methanol steam reforming reaction, it is examined that there are several other products formed during the process which should be counted for consideration. Here the product mixture is comprising of hydrogen, carbon dioxide, and a small quantity of carbon monoxide other than non-reacted water and methanol. Thus it is imperative to minimize the amount of carbon monoxide formed where its upper limit must take a figure lower than 10 ppm. If not, the anodic catalyst of the fuel cell might be deteriorated. Thus this manifests the significance of having a good catalyst performance in the reaction. The ideal catalyst should have a higher activity to obtain a higher yield of hydrogen, a higher selectivity to have negligible amounts of carbon monoxide, and finally should possess long-term stability (Sari & Sabziani, 2017).

There are two categories of catalysts generally used in methanol steam reforming reactions, they are copper-based catalysts and group VIII-X catalysts. Here copper-based catalysts are normally inexpensive and active while the latter group provides enhanced thermal stability and long-term stability. Most often copper-based catalysts are favored based on the economic sense. However, thermal sintering, coke deposition, and change in the oxidation state cause deactivation of these catalysts. At temperatures above 300 °C, the copper crystallites readily tend to undergo sintering which suggests that the operational temperature of conventional Cu-based catalysts should always be kept below 300 °C. Further, the literature claims that the sintering of Cu also might cause due to the concentration of steam (Rameshan, 2012). And also there might be a decrease in activity and variations in selectivity due to Cu(0)/Cu(I) oxidation state change (Rameshan, 2012). Thus it is required to modify the copper-based catalyst such that it is capable of providing higher hydrogen production at lower reaction temperatures without undergoing massive deactivation.

As mentioned above Cu-based catalysts are often used in methanol steam reforming processes. It is reported that the status of copper effects on the functionality of copper-based catalysts. To have a catalyst functioning with high activity, the catalyst should possess enhanced dispersion of small particle sized copper with high metal surface area (Sun, Metcalfe, & Sahibzada, 1999). Thus literature reveals several approaches that have been carried out in augmenting the activity of these catalysts. Here some researches study on the effect of adding promoters while others investigate how

the catalyst preparation method affects its final activity (Ogawa & Koteka, 1978). Further several authors claim that each step in the catalyst preparation method is capable of affecting the general properties of the catalyst. That means similar catalysts prepared by various methods may carry specific and unique catalytic properties.

This work investigates two modifications done during the catalyst preparation to increase the activity at low temperatures 1) Support modification 2) Enhancement of dispersion of active metals on the catalyst support.

Generally, γ - Al_2O_3 is well known for being a good support for catalysts due to its high surface area and thermal stability. Yet literature suggests that Copper-ceria based catalyst is known to improve both activity and stability of the catalyst for MSR through high oxygen storage capacity (Wang, Tsai, & Huang, 2002). Therefore, Ce is used as a dopant in the support of Cu-Zn/ γ - Al_2O_3 catalyst in this study. The amount of Ce will be kept at a low percentage to keep the high surface area and low cost. However, it may cause the segregated phase of CeO_2 to be separated from the Al_2O_3 framework instead of the formation of Ce- Al_2O_3 in the Al_2O_3 framework. This may happen due to poor Ce distribution during the support preparation. The literature reported that the application of an external magnetic field to a dilute solution can cause to have variations in the movement of ions during their process of gelation (Fujiwara, Chie, Sawai, Shimizu, & Tanimoto, 2004). Therefore, magnetic inducement was applied to control the composition and the dispersion of Ce into Al_2O_3 framework during sol-gel support preparation process. This modification might improve the homogeneity of Ce dopant in the support framework and prevent the formation of segregated CeO_2 .

The most common catalyst preparation method for industrial-scale is impregnation, but the metal dispersion is limited due to uncontrollable metal movement (Marquez, 2017). Here, Cu and Zn must be located together on the support for the catalyst to be in the most active form. However, this phenomenon cannot be manipulated under normal conditions. Therefore, sol-gel technique could improve the metal dispersion, and the magnetic inducement could influence the movement of Cu and Zn ions within the support (Lei, Nie, Fei, & Hou, 2012). Thus the well-dispersed active metals on the modified support together may provide an attractive development of low-cost Cu-Zn based catalyst. This modified catalyst might be active at low temperatures giving a high yield of H_2 from MSR.

1.2 Objective

The main goal of this research is to modify Cu-Zn based catalyst to get higher hydrogen production yield at lower reaction temperatures from methanol steam reforming reaction. Thus this study focusses on support modification and enhancing dispersion of active metals on the catalyst support. The objectives of this research study are listed as follows:

1. Support modification using CeO₂-doped Al₂O₃ support and to investigate the effect of magnetic inducement during the preparation of CeO₂-doped Al₂O₃ support.
2. To investigate the effect of magnetic inducement during the introduction of Cu-Zn active metals on the γ -Al₂O₃ support and CeO₂-doped Al₂O₃ support.

1.3 Scope of the study

This study focuses on the catalytic activity improvement of Cu-Zn based catalysts for methanol steam reforming reaction by support modification and enhancing Cu-Zn active metal dispersion on the support. Thus the scope is divided into two parts based on the two different approaches.

1.3.1 Support modification

CeO₂-doped Al₂O₃ supports (Ce-Al₂O₃) with 5mol% of Ce loading are prepared by sol-gel method with the application of different magnetic pole arrangements; North-North (N-N), North-South (N-S) and no magnetic inducement. Then 5wt% Cu-Zn active metals are introduced into these prepared supports by sol-gel method without applying any magnetic field inducement. The catalytic activity tests are conducted in a tubular quartz reactor within the temperature range of 200–300 °C at atmospheric pressure. The extent of Ce dispersion in γ -Al₂O₃ framework for each support is evaluated by H₂-TPR chemisorption technique. While the performance of catalysts is evaluated in terms of gas production by gas chromatography analyzer.

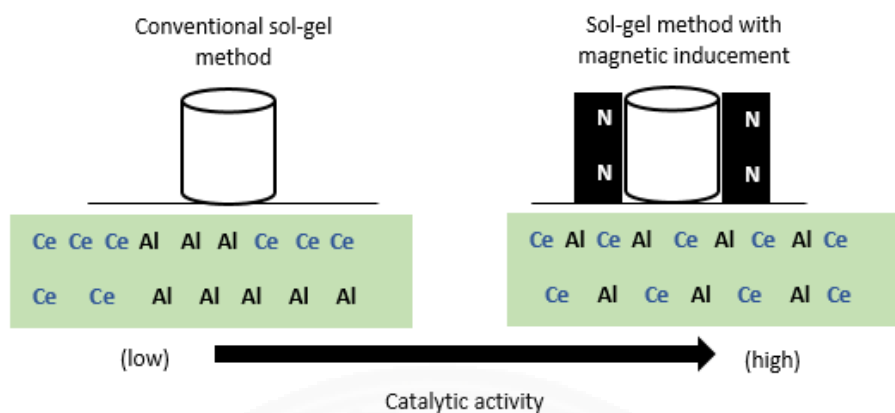


Figure 1.1 Graphical summary of CeO₂-doped Al₂O₃ support modification.

1.3.2 Enhancement of active Cu-Zn metal dispersion on the support

Here 5wt% Cu-Zn active metals are introduced into γ -Al₂O₃ support and previously prepared CeO₂-doped Al₂O₃ supports by applying different magnetic pole arrangements like (N-N), (N-S) and no magnetic field during its sol-gel preparation method. The catalytic activity tests for MSR are conducted in a tubular quartz reactor within the temperature range of 200–300 °C at atmospheric pressure. The uniformity of Cu-Zn dispersion on γ -Al₂O₃ framework and CeO₂-doped Al₂O₃ framework for each catalyst is evaluated by H₂-TPD chemisorption technique. While the performance of catalysts is evaluated in terms of gas production by gas chromatography analyzer.

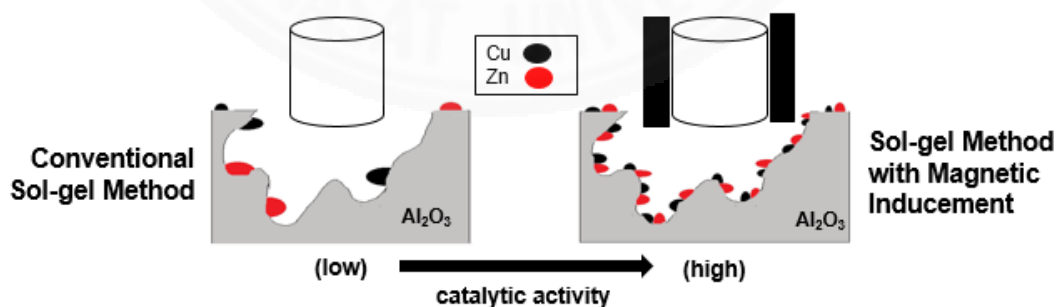


Figure 1.2 Graphical summary of Cu-Zn metal dispersion on γ -Al₂O₃ support.

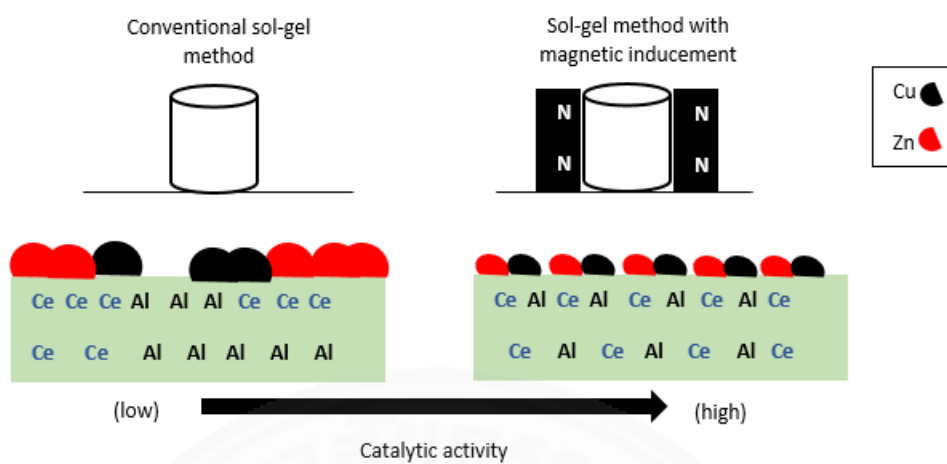


Figure 1.3 Graphical summary of Cu-Zn active metal dispersion on CeO₂-doped Al₂O₃ support.

CHAPTER 2

REVIEW OF LITERATURE

2.1 Hydrogen production

Hydrogen gas can be produced through various methods, out of them the four basic processes are electrochemical, thermochemical, biochemical, and photolysis methods (Yang & Liao, 2007).

In the electrochemical process, it incorporates the utilization of an electric current in splitting water molecules into hydrogen and oxygen in a specialized chamber commonly known as an electrolyzer. Such produced gas is considered as clean energy since it possesses nil emission of greenhouse gas. Anyway, during the process of electricity generation, it still can have an emission of hazardous pollutants. Thus in modifications, to have complete zero emission of greenhouse gases and pollutants, clean electricity generation systems are developed as nuclear and renewable energy (wind and solar) (Lorenz, Friedrich, Armbrüster, Klötzer, & Penner, 2013).

Heat and chemical reactions from organic chemicals like coal, biomass, and natural gas are utilized in hydrogen generation in thermochemical processes. Here there is a possibility of releasing hydrogen out of their chemical structure in form of hydrogen molecules or hydrogenated compounds such as water because of the combination of closed chemical cycle and heat that occurred during the process. The four significant processes encountered in this category are biomass-derived liquid reforming, biomass gasification, methane reforming and coal gasification based on the amount of hydrogen yield obtained (Tsai, Wang, Shen, & Yeh, 2011).

Biochemical processes are also often used in hydrogen production because of its long-term potential and low-carbon generation. Here microbes such as bacteria and microalgae are involved in the digestion of organic matters such as raw biomass and wastewater. Further hydrogen can be obtained as a byproduct of the fermentation process. Based on the type of microbes and pathways incorporated in the fermentation process it can be carried out either with light or without light (Danwittayakul & Dutta, 2012).

In the photo-electrochemical (photolysis) process, the water molecule is split into hydrogen and oxygen with the utilization of direct solar energy. And then through a semiconductor solar energy is transformed into chemical energy. Since it releases no or low greenhouse gas, this process has the potential in long-term sustainability with minimum environmental impacts (Danwittayakul & Dutta, 2013).

Other than these significant processes, there are plenty of hydrogen production methods used in real applications. Some of the other common methods used in hydrogen production are summarized in Table 2.1.

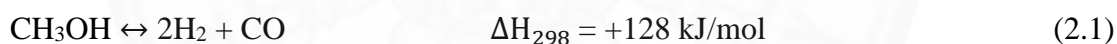


Table 2.1 Overview of hydrogen production methods by primary energy and material source(Acar & Dincer, 2014).

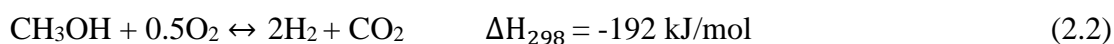
Method	Source		Brief Description	Ref.
	Primary Energy	Material		
PV electrolysis	Photonic	Water	PV panels are used in generation of electricity	(Jin, Lu, Liao, Guo, & Zhang, 2010)
Photo electrochemical method			A hybrid cell simultaneously produces current and voltage upon absorption of light	(Galvita, Messerle, & Ustimenko, 2007)
High temperature electrolysis	Electrical + thermal	Water	Electrical and thermal energy are used together to drive water splitting at high temperatures	(Doenitz, Schmidberger, Steinheil, & Streicher, 1980)
Plasma arc decomposition		Fossil fuels	Cleaned natural gas is passed through plasma arc to generate H ₂ and carbon soot	(Gaudernack & Lynam, 1998)
Photo catalysis			Water is split into H ₂ by using the electron-hole pair generated by the photo catalyst	(Acar & Dincer, 2014)
Dark fermentation	Biochemical	Biomass	Biological systems are used to generate H ₂ in the absence of light	(Das & Veziroglu, 2008)
Coal gasification			Conversion of coal into syngas	(Y. Li, Guo, Zhang, Jin, & Lu, 2010)
Fossil fuel reforming			Fossil fuels are converted to H ₂ and CO ₂	(Holladay, Hu, King, & Wang, 2009)
Biophotolysis	Photonic + Biochemical	Biomass + Water	Biological systems (microbes, bacteria, etc.) are used to generate H ₂	(Nath & Das, 2004)

2.2 Hydrogen production from methanol

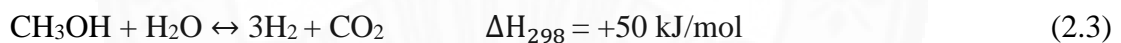
One of the most significant and convenient methods of producing hydrogen is the reforming of hydrocarbons and alcohols. Based on the unique chemical and physical properties of methanol like low cost, high energy density, and easy transportation it is often considered as one of the most used liquid fuels for hydrogen production. The presence of one Carbon atom makes methanol to be the simplest form of alcohol for reforming. Since methanol does not have a strong C-C bond, it helps the reforming to be carried out at lower reaction temperatures like (200–300) °C. This temperature range is very low comparing to reforming temperatures of other alcohols such as methane, which is normally reformed at a temperature above 500 °C. While for ethanol the reforming temperature lies around 400 °C. Further, the literature says that despite being highly toxic and miscible in water, methanol has the favor of existing in the liquid state at atmospheric conditions. And also methanol is biodegradable and has higher hydrogen to carbon ratio. Here Decomposition, Partial Oxidation, and Steam Reforming are the significant processes incorporated in hydrogen production through the conversion of methanol (Agarwal, Patel, & Pant, 2005).



As shown in Equation 2.1, since decomposition reaction acquires only methanol as the feedstock or raw material, it becomes the simplest form of methanol conversion. Anyway, the process needs a lot of operational energy since the reaction itself is actively endothermic. Further, the literature reveals that the mixed product gas is comprised of 67% of hydrogen and a carbon monoxide amount of 33%. Where the greater percentage of CO needs the installation of a CO clean-up chamber in fuel cell systems. In industrial level, the CO clean-up chamber is considered as one of the most complicated segments in a fuel cell system. Thus based on these disadvantages, it can be manifested that the methanol decomposition is inconvenient to be actively used in applications of fuel cells (Papavasiliou, Avgouropoulos, & Ioannides, 2005).



Partial oxidation reaction as shown in Equation 2.2 is a way fast and exothermic process compared to the decomposition method. Since the reaction itself is exothermic, there is no need of supplying additional energy for the process to have happened. Yet, designing a suitable reactor requires extra consideration of how the exothermic behavior of the reaction affects the heat and temperature profiles. The literature claims that the rapid increment of temperature may give rise to hot spots. Then these cause sintering of the metal particles and tend to have deactivation of the oxidation catalyst (L. Wang, Liu, Chen, Cao, et al., 2007). When pure oxygen is used in the feed mixture, a product mixture comprises a hydrogen concentration of 67% can be obtained. But in the real scenario, oxygen uptake needed for the automotive fuel cell applications are obtained from surrounding air. Since atmospheric air contains a higher percentage of nitrogen, there is a possibility that the product gas mixture being diluted with nitrogen. Thus in such a fuel cell system, the hydrogen content may reduce up to 41% which may badly influence the generation of electricity (McGuirk, Ledieu, Gaudry, De Weerd, & Fournée, 2014).



It is clear according to Equation 2.3 that the steam reforming of methanol (SRM) can also be considered as a reverse reaction of synthesis of methanol. When comparing with the previous two methods, SRM becomes the most convenient method of hydrogen production through methanol conversion. SRM gives a product gas mixture with a high hydrogen content of 75%. While the reaction itself has a high selectivity of carbon dioxide. This is an endothermic reaction where the required energy can be provided through a catalytic burner device (Latorre, Ubieta, Royo, & Romeo, 2006). Since this process is comprised of high values in methanol conversion, high yields of hydrogen, and moderate reaction conditions, it is subjected to intense studies and researches.

Apart from original SRM, the literature reveals that the combination of partial oxidation and steam reforming of methanol is also an effective process to be carried out in hydrogen production (Udani, Gunawardana, Lee, & Kim, 2009). The significant advantage of the modified latter process is that reaction itself has the possibility of

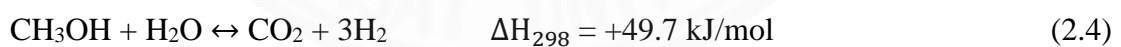
fulfilling the heat requirement (auto thermal reaction). However, the obtained product gas mixture has a lower hydrogen concentration with a low methanol conversion compared to the original SRM reaction (Papavasiliou, Avgouropoulos, & Ioannides, 2007). Thus based on all these details, this study focuses on improving hydrogen production through methanol steam reforming reaction.

2.3 Methanol steam reforming reaction

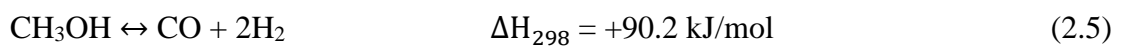
In reforming reactions, the molecular structure of hydrocarbons and alcohols is rearranged making a new molecule. This is the process most often used in industrial level to obtain hydrogen through direct synthesis using different reactants. Here each hydrocarbon carries unique properties and requirements to have better hydrogen yields (Agrell et al., 2003).

Out of many hydrocarbons and alcohols, methanol is one of the most productive feedstock in hydrogen production based on its properties like low boiling point (64.8 °C), low purchasing cost, high availability, and having a high H:C ratio. Thus the use of methanol steam reforming products (MSR) in fuel cells, avoids hydrogen storage problems and the cost of producing sustainable energy. The following describes the overall methanol steam reforming reaction consists of methanol decomposition (MD) and water gas shift (WGS) reactions.

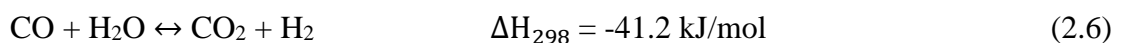
Methanol steam reforming:



Methanol decomposition:



Water-gas shift:



Here methanol decomposition (MD) reaction becomes highlighted in internal combustion engine feed applications because it may give rise to coking problems. Other than that, during the occurrence of methanol decomposition, it may lead having

unnecessary side reactions which may produce small quantities of methyl formate, dimethyl ether, formaldehyde and, etc (Amiri & Moghaddas, 2016).

Dehydration:



Methanation:



Dehydration:



Decomposition:



Dehydrogenation:



Formaldehyde synthesis:



Carbonation:



Here to ensure high hydrogen yield, the selected catalyst must have a higher activity and stability for steam reforming reaction and water gas shift reaction, at temperatures lower than its product gas mixture (Papavasiliou et al., 2005). Further, the literature reveals that the process of converting methanol to CO_2 and H_2 is inconvenient since CO_2 acts as a diluent gas rather than an energy carrier. And also MSR suffers less from coking problem compared to methanol decomposition (Agarwal et al., 2005). Thus by considering all these facts, it is highly imperative to have a highly active catalyst that provides more hydrogen yield with less selectivity for carbon monoxide.

2.4 Catalysts for methanol steam reforming reaction

Normally catalytic reactions are a type of chemical reaction that is achieved with the aid of a substance called a catalyst. The catalyst is a substance that accelerates the rate of a chemical reaction by decreasing the relevant activation energy. The

literature says that catalyst acts as a part of the chemical reaction which does not undergo any consumption during the process yet subjected to deactivation due to some additives (catalyst poisons). There are two basic categories of catalysts they are heterogeneous and homogeneous catalysts. Catalytic reactions that take place in one phase are homogeneous catalysis while reactions involve two or more various phases are called heterogeneous. Apart from the very preliminary properties of catalysts like selectivity, stability, and activity, catalysts should be reproducible, re-generable economical, and should possess strong mechanical and thermal stability to be used vividly in industrial applications (Oguchi et al., 2005). In recent studies, they have examined the effect of active metals, supports, and promoters in providing good catalytic performances.

The active metal can be categorized into 2 major groups; noble metal (group 8-10) and non-noble metal catalysts. The noble metal catalysts Palladium (Pd), Platinum (Pt), Rhodium (Rh), and Ruthenium (Ru) are well known for their high stability and approximately similar selectivity same as non-noble metal catalysts. However, the price of noble metals is high, and the availability is low therefore, making them less suitable for commercializing. Therefore, Cu based catalyst is used as the low-cost alternative to noble metals (L. Wang, Liu, Chen, Liu, et al., 2007).

Cu-based catalyst is the most focused one because catalysts with a high composition of Cu will lead to higher conversion and selectivity. However, there are several significant drawbacks of Cu-based catalysts such are deactivation, pyrophoricity, and sintering at high temperatures (more than 400 °C). Hence, the conventional Cu-based catalysts should not be used in the operation temperature beyond 400 °C. In addition, Cu tends to exist in Cu^{2+} form, but the most active form is the Cu^+ . Therefore, using Cu alone as active metal is inadequate for methanol steam reforming, but modifying it with other metals is more extensive. In methanol steam reforming processes, the commonly used materials with Cu-based catalysts for hydrogen production are Zn as the co-metal active site. The role of Zn is to be an electron donor (lower reduction potential) for transferring an electron to Cu^{2+} to reduce to Cu^+ . For this to happen, Cu and Zn must be located together to achieve the most efficient form for this catalyst (Kowalik & Go, 2013).

Several catalyst preparation methods can be incorporated in making Cu-based catalyst, some of the most used methods are sol-gel, precipitation, impregnation, oxalate gel co-precipitation, and hydrothermal synthesis. These preparation methods can effect on the characteristics of the final catalysts. Literature reveals that the activity of Cu-based catalysts can be evaluated by its status of copper. Where high active Cu-based catalysts possess high dispersions of copper and relatively high specific copper surface area (Sá et al., 2010). The following Table 2.2 lists several Cu-based catalysts evaluated for methanol steam reforming reaction in previous studies.



Table 2.2 Reaction conditions and hydrogen yield for methanol-steam reforming reaction (MSR) by various Cu-based catalysts.

Catalyst	Catalyst Preparation Method	Reaction Conditions			Methanol Conversion (%)	Hydrogen Production (%)	Reactor	Ref.
		Temperature (°C)	Pressure (atm)	H ₂ O:Methanol Ratio				
Cu/ZrO ₂	IMP	260	1	1.3	10	≤ 10	FBTR	(Jeong et al., 2006)
Cu/Zn		230			≤ 10	≤ 10		
Cu/Zn		300			37	20		
Cu/ZrO ₂	CP	260			60	40		
Cu/Zn	IMP-BD	230	1	1.3	50	35	FBTR	(Jakdetchai, Takayama, & Nakajima, 2005)
Cu/ZnO	CP	250	1	1.3	46	38	FBTR	(Shishido, Yamamoto, Morioka, Takaki, & Takehira, 2004)
Cu/ZnO	HP				94	65		
Cu/ZnO/Al ₂ O ₃					96	70		

IMP: impregnation; CP: Co-precipitation; IMP-BD: modified impregnation with 1,3-butanediol; HP: homogeneous precipitation; FBTR: fixed bed tubular reactor

Catalyst	Catalyst Preparation Method	Reaction Conditions			Methanol Conversion (%)	Hydrogen Production (%)	Reactor	Ref.
		Temperature (°C)	Pressure (atm)	H ₂ O:Methanol Ratio				
Cu/Zn/Zr/Al	SQ	260	1	1.3	61	48	FBTR	(Zhang et al., 2013)
	CI-NP				63	49		
	CI				65	52		
Cu/Zn/Al ₂ O ₃	commercial				60	45		
Cu-Mn	OGCP	260	1	1.2	59	47	FBTR	(Rakoczy, Nizioł, Wieczorek-Ciurowa, & Dulian, 2013)
Cu-Mn	CP				65	50		
Cu-Mn spinel	SRG				90	60		
CuO/ZrO ₂	PTSG	260	1	1.1	92	65	FBTR	(Patel & Pant, 2006)
CuO/ZnO/Al ₂ O ₃	commercial	250			90	63		
Cu/Zn/Zr/Al	WT	260	1	1.3	60	45	FBTR	(Matsumura & Ishibe, 2009)
Cu/Zn/Zr/Al	CP				95	66		
Cu/ZnO	CP	240	1	1.3	43	30	FBTR	(Patel & Pant, 2006)
Cu/ZnO					48	32		

SQ: sequential impregnation; CI-NP: co-impregnation with nanoparticle precursor; CI: co-impregnation; OGCP: oxalate gel co-precipitation; CP: co-precipitation; SRG: soft reactive grinding technique; PTSG: polymer template sol-gel method; WT: wet impregnation; FBTR: fixed bed tubular reactor

2.5 Supports for Cu-based catalysts

Another factor that can affect the catalytic functionality of a catalyst is the support. For mono-function catalysts, the reaction occurs only at the active metal sites (Hou, Zhang, Chen, Wang, & Cai, 2015). However, the reactants can be adsorbed on both the active metal and the support for bi-functional catalysts. Some types of supports can enhance the reaction mechanism such as the ability for H₂O splitting or C-C and C-H bond rupture (He, Yang, Wang, Zhao, & Duan, 2012). Some supports, such as CeO₂, act as oxygen species suppliers for chemical reactions which eventually enhance the activity of the catalyst.

One of the most famous supports for MSR is Al₂O₃ because of its relatively high surface area for active metal, and its high thermal and chemical stability. However previous studies on methanol steam reaction show that it is better to have a proper functioning mixed oxide as the support rather than conventional pure Al₂O₃.

Other than Al₂O₃, ceria is also one of the interesting supports used for MSR due to its unique property of oxygen storage and release system. This in turn leads to the presence of highly active oxygen for the oxidation of hydrocarbons (Ebiad, Abd El-Hafiz, Elsalamony, & Mohamed, 2012). Ceria can also disperse and stabilize the active metal by using the defects on its surface as the anchors (Hou et al., 2015).

2.5.1 Structure of Al₂O₃

γ -alumina (γ -Al₂O₃) is the most frequently used support in catalysts for methanol steam reforming reactions. Because of phase compositions, local microstructure, and surface chemical compositions of γ -Al₂O₃, it possesses a higher surface area and comparatively high thermal and chemical stability. These characteristics aid the support to be made to an active catalyst which provides adequate amounts of H₂ along with an acceptable low selectivity to CO (Myronyuk, Mandzyuk, Sachko, & Gun'ko, 2016). There are lots of research studies that have analyzed the structural characterizations of γ -Al₂O₃ through several techniques such as, X-ray diffraction, and transmission electron microscopy (TEM) (Trueba & Trasatti, 2005).

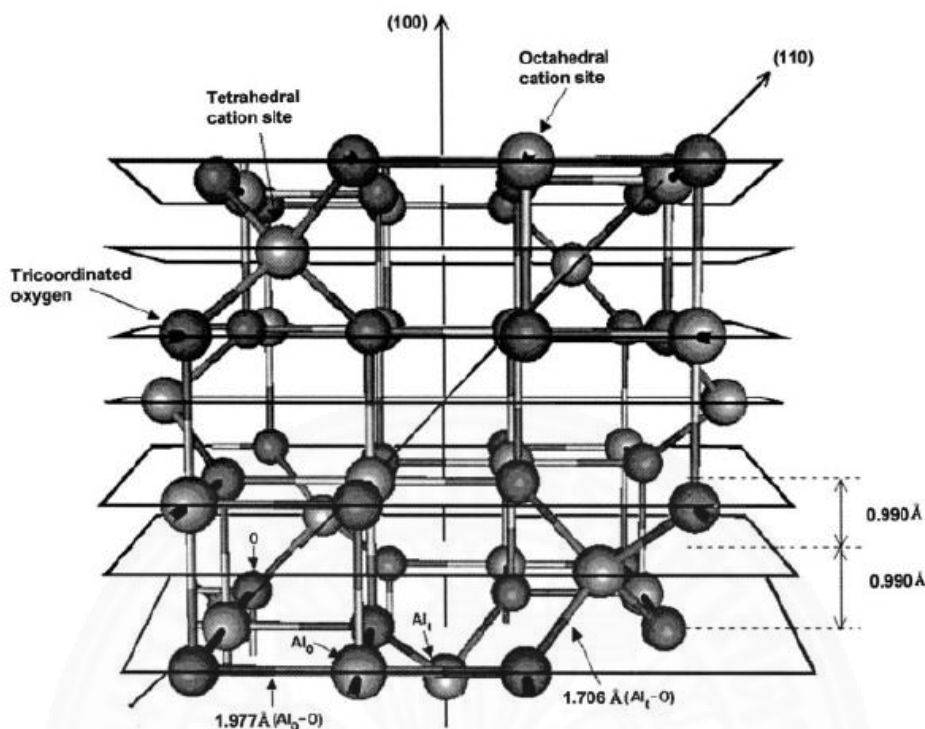


Figure 2.1 Experimental cubic Al_2O_3 spinel-type unit cell (Trueba & Trasatti, 2005).

Figure 2.1 shows the spinel-type unit cell of cubic $\gamma\text{-Al}_2\text{O}_3$, where the trivalent Al cations provide the defective nature. Here the magnesium atoms in the MgAl_2O_4 spinel are replaced by Al atoms. Further, studies reveal that Al atoms are filled in octahedral and tetrahedral sites while the oxygen lattice is built by layers of oxygen atoms arranged in the shape of cubic-closed packing (Myronyuk et al., 2016).

The significant difference between the $\gamma\text{-Al}_2\text{O}_3$ structure and the MgAl_2O_4 spinel structure is the number of atoms involved in building up the unit cell. Thus as illustrated in Figure 2.1, the MgAl_2O_4 spinel structure is comprised of 8 Magnesium atoms placed in tetrahedral sites, 16 aluminum atoms fitted in octahedral sites, and 32 oxygen atoms in the oxygen lattice summing the total of 56 atoms. While the $\gamma\text{-Al}_2\text{O}_3$ structure is consists of 24 oxygen atoms, 16 aluminum atoms, and 2 cation vacancies which are randomly located either in octahedral or tetrahedral sites (Myronyuk et al., 2016).

These vacancies in the spinel structure of $\gamma\text{-Al}_2\text{O}_3$ may increase the opportunity for heteroatoms to be doped into the Al_2O_3 framework by insertion or replacement. The

result of the insertion or replacement of heteroatoms with different valence and/or different atomic sizes in Al_2O_3 framework is a defect formation. The defects in the support framework allow the formation of oxygen vacancies which alter the metal-support interaction and increase catalytic activity (Myronyuk et al., 2016). In recent researches, alumina is studied more often as the basic component of catalysts by adding ZrO_2 , TiO_2 , SiO_2 , La_2O_3 , CeO_2 , etc. as doping sources, to enhance the properties of Al_2O_3 supports that provides the benefit towards the MSR reaction.

2.5.2 Properties of CeO_2

Cerium oxide and CeO_2 containing materials can be considered as an intense source of catalysts and as an electronic and structural promoter of various heterogeneous catalytic reactions. Depending on this significance, three-way catalysts incorporate CeO_2 as a prominent compound to treat the exhaust gas from vehicles. Following are few of the prominent advantages of using Ce in three-way catalysts, (a) has a strong metal-ceria interaction (b) is capable of changing vice versa from Ce^{4+} (CeO_2) to Ce^{3+} (Ce_2O_3) under redox conditions (P. Li, Chen, Li, & Schwank, 2018). Thus following listed are some of the secondary benefits of CeO_2 which might influence on the performance of catalysts in distinct ways (Damyanova, Pawelec, & Arishtirova, 2008).

- 1) Effects on the dispersion and distribution of supported metals
- 2) boost up the water gas shift reaction and steam reforming reactions
- 3) thermal stability of the support is enhanced
- 4) undergo reduction and oxidation of noble metals
- 5) storage and release of oxygen, hydrogen, and sulfur
- 6) formation of surface and bulk vacancies
- 7) formation of inter metallic M-Ce compounds

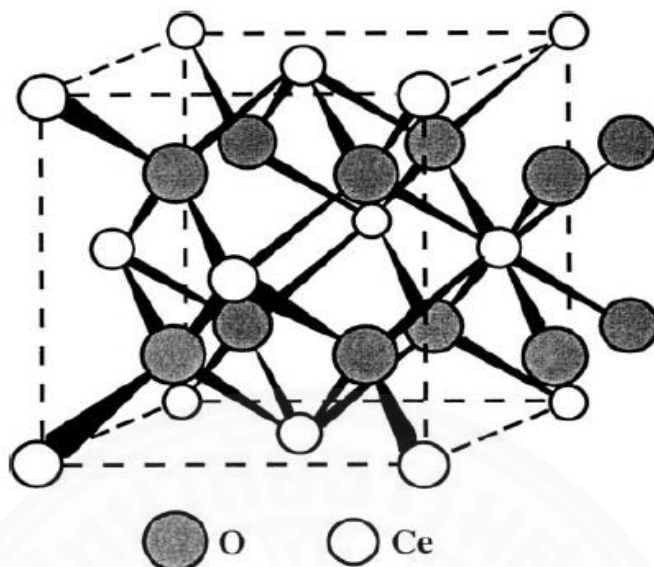


Figure 2.2 The fcc unit cell of CeO₂ with the fluorite structure (Trovarelli, 1996).

Cerium oxide is built up with fluorite (CaF₂) structure, where metal atoms are composed in a cubic closed-packed array. Here oxygen atoms are placed up in tetrahedral holes. When CeO₂ is subjected to reduction at higher temperatures, it has the ability to form CeO_{2-x} (0 < x < 0.5) oxides which are oxygen deficient and nonstoichiometric. In the meantime, reduction of CeO₂ at lower temperatures (T < 723 K), gives rise to a sequence of distinct components. Although CeO₂ losses a significant amount of oxygen from its lattice structure and form large number of oxygen vacancies, still CeO₂ is capable of maintaining its fluorite crystal structure. And also by exposing the formed sub-oxides in an oxidizing atmosphere, they can be re-oxidized to CeO₂ (Martí, Ferná, Conesa, & Soria, 2000).

There are researches that have studied the reductive nature of CeO₂, supported CeO₂, and M/CeO₂ compounds and their importance in catalysis. For these analysis, they have used several techniques such as chemisorption, temperature-programmed reduction and desorption, Raman spectroscopy, X-ray photoelectron spectroscopy (XPS), transmission electron microscopy (TEM), thermogravimetry and many more (Yao, 1984). Thus the following sections elaborates the reductive nature of ceria and related compounds once H₂ and CO are used as chemisorption gases.

2.5.2.1 Interaction with Hydrogen

As mentioned earlier there are massive amount of details about the redox nature of CeO_2 which have been gathered through the results of temperature-programmed reduction (TPR) analysis done at both low and high temperatures having interactions with H_2 .

According to Figure 2.3, the H_2 -TPR profile of pure CeO_2 , defines two prominent peaks, approximately at 770 K and 1100 K temperatures which illustrates the reduction of CeO_2 to Ce_2O_3 . Here the reduction of the most easily detachable and reducible surface oxygen of CeO_2 give rise to the first peak at low temperature (770 K). Whereas the removal of oxygen located in bulk layers of CeO_2 describes the peak at high temperature 1100 K (Hickey et al., 2001).

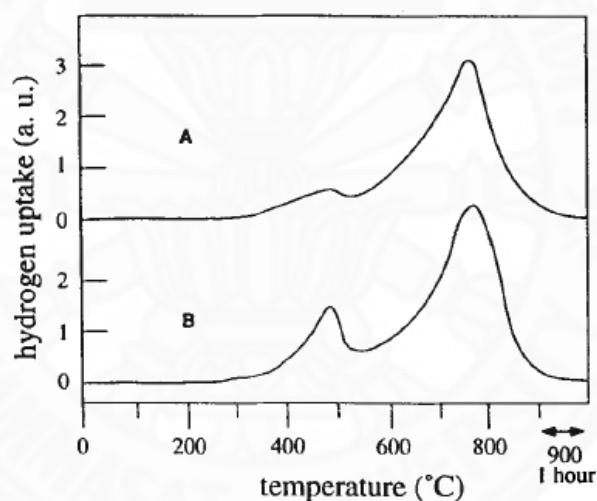


Figure 2.3 TPR of CeO_2 samples. (A) CeO_2 BET surface area $1 \text{ m}^2/\text{g}$; (B) CeO_2 BET surface area $10 \text{ m}^2/\text{g}$ (Hickey et al., 2001).

There is another simple model which describes the correlation between surface area and H_2 -TPR signals of CeO_2 . This model assumes that the ceria surface is built up of adjoining oxygen ions, where the number of oxygen ions can be easily calculated through cubic particles. By assuming that the reduction of CeO_2 happens through the removal of quarter of the surface oxygen ions, it is easy to calculate the H_2 consumption relevant to the surface area of CeO_2 . Thus to modify this model, literature claims that

they had employed low surface area CeO₂ samples (not greater than 27 m²/g). Yet the model was unable to provide decisive functionality of CeO₂ samples which had a surface area higher than 13 m²/g. The same restriction carries for CeO₂ samples with high surface area (Bouly, Chandès, Maret, & Bianchi, 1995). Therefore, a much definite model was later developed to study the H₂-TPR profiles of CeO₂ samples with different textures (Hak et al., 2016). In this study the researches have used CeO₂ samples with a range of different surface areas, and the developed model was capable of providing a better correlation between amount of H₂ consumed and BET surface area from the very first peak obtained. Further they have claimed that the amount of H₂ consumed varies linearly with the surface area. This relationship claims that first the surface oxygen in CeO₂ gets reduced and then progressively followed to bulk oxygen (Martı et al., 2000). Despite all these details still there is no precise model or correlation to explain H₂-TPR analysis for CeO₂ compounds with higher surface area. Thus following describes the general kinetic model for reduction of ceria through H₂-TPR analysis.

- 1) H₂ is dissociated giving hydroxyl groups.
- 2) Anionic vacancies are formed and adjacent cations get reduced.
- 3) Water gets desorbed by recombining hydroxyl group and hydrogen.
- 4) Surface anionic vacancies get diffused into the inner bulk layers.

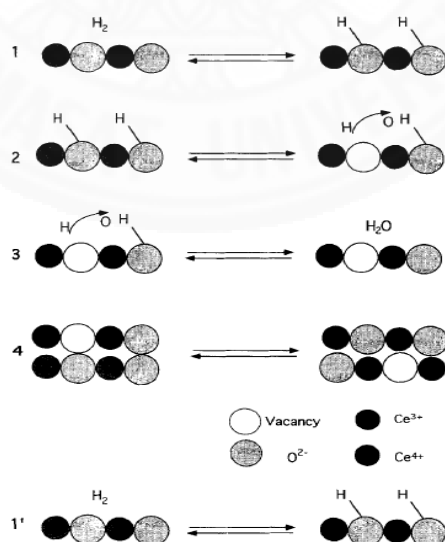


Figure 2.4 Pathway proposed for CeO₂ surface reduction (El Fallah et al., 1994).

Literature claims that surface step is the rate determining step in this model which clearly describes the effect of surface area on the kinetics of the reaction. Further it describes that inauguration of reduction process immensely depend on the sample surface area and the reduction of bulk layers only commence once all the surface sites are completely reduced. And this reduction process is then advantaged by the comparatively high movement of oxygen into the lattice of CeO₂. And also results by FT-IR analysis have shown that once CeO₂ is treated with H₂ it forms hydroxyl groups through dissociative chemisorption of H₂ (step 1). And also here process of reduction is related to the formation of oxygen vacancies which happens in step 2 (Damyanova et al., 2008).

On the other hand, there is another model which interprets a complete contrast pathway, of not including the formation of oxygen vacancies during reduction of ceria in its first platform. Here in the first stage an outgassing technique accompanies an easy re-oxidation. Which is then followed by formation of Ce³⁺ (Yao, 1984). And also the researches have concluded that H₂ adsorption obtained through this model carries only the surface area of ceria eliminating circumstances of expanded dissolution of H₂ into the inner layers of ceria (Cunningham et al., 1990).

X-ray diffraction technique can also be incorporated to examine the phase changes happened during CeO₂ reduction using H₂ at mild and higher temperatures. Once CeO₂ reduction is done using H₂, the hexagonal Ce₂O₃ and CeO_{1.82} are not to be observed at temperatures upto 1073 K as described earlier. Here once CeO₂ is treated with H₂, Ce³⁺ is formed and the lattice structure gets expanded due to larger atomic size of Ce³⁺ compared to Ce⁴⁺ (1.14Å vs. 0.97Å) which eventually shifts the main diffraction peaks correspond to (111) (200) (220) (311) reflections (Fornasiero et al., 1995).

Further the literature reveals that, TPR profiles of supported CeO₂ (such as on SO₂ or Al₂O₃) gets alternated based on the nature of the interaction of the two oxides. Here TPR profiles of supported CeO₂ compounds interpret some distinct characteristics other than the ordinary features. Here studies claim that shape of the TPR graph depends on the crystallite size of the deposited CeO₂. Further, only compounds with higher CeO₂ loadings, show H₂ uptake responsible for bulk oxygen removal. Results through XPS

and Raman spectroscopy has shown that CeAlO_3 species are formed in compounds with low CeO_2 loadings during reduction of surface oxygen at lower temperatures. And also amount of loaded CeO_2 on the compound affects for the shift of 2 peaks in TPR profile. Here decreased amount of CeO_2 loading exhibits a shift for the high temperature signal towards the low temperature peak. Meanwhile the low temperature peak experiences only small deviations around 700 K (SAKAMOTO et al., 2002). Several studies have revealed that once the CeO_2 loading decreases, the percentage of CeO_2 being reduced within the temperature range of 800-1200 K gets increased. Thus they have studied Pd/Ce/ Al_2O_3 , Pt/Ce/ Al_2O_3 , and Rh/Ce/ SiO_2 supports and have declared that the extent of reduction of surface ceria within low temperatures is affected by the loading of CeO_2 and degree of dispersion of CeO_2 on the support. Thus likewise the following Figure 2.5 illustrates that CeO_2 gets dispersed well on silica surface once the CeO_2 loading is low in the presence of hydrogen (Shi et al., 2002).

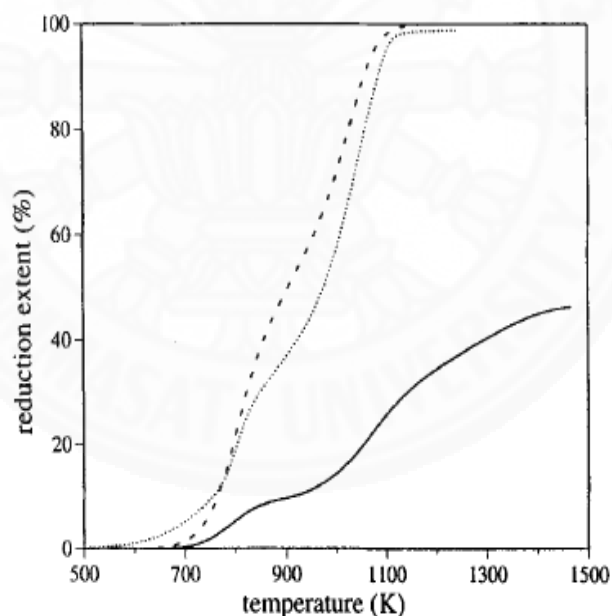


Figure 2.5 Extent of CeO_2 reduction vs. temperature for CeO_2 (-), CeO_2 (28.4%)/ SiO_2 (...), and CeO_2 (1.6%)/ SiO_2 (---) as determined from TPR analysis (De Leitenburg et al., 1997).

2.5.2.2 Interactions with Carbon Monoxide

Other than hydrogen, carbon monoxide is also a useful probe for characterization through adsorption on metal oxide surfaces. Thus there are number of studies that have investigated the CO-ceria interactions. Literature suggests that once CO is adsorbed on ceria surface, surface oxygen of CeO₂ gets reduced forming oxygen vacancies (Trovarelli, 1996).



■ : oxygen vacancy

Studies say that carbon monoxide is a more attractive probe gas than H₂ for ceria. Once CO is adsorbed on CeO₂, it undergoes rapid reduction at room temperatures and CeO_{1.86} oxides are observable at temperatures around 673 K. Here the textural and morphological features of CeO₂ containing samples play a vital role in determining the extent of reduction of CeO₂ by CO. Once CO-TPR profiles are evaluated it can be stated that the reduction process becomes difficult once the CeO₂ lattice becomes more perfect (Boaro, Vicario, De Leitenburg, Dolcetti, & Trovarelli, 2003).

Performing TPR using CO mixed He gas mixture has the benefit of diffusing into the bulk particles where the use of conservative CO-TPR is lack of this property. Thus here reduction happens through a chemical pump effect where it causes oxygen to be diffused up to the surface and subsequent displacement with oxygen vacancy formation (Oguchi et al., 2005).

2.5.2.3 Adsorption and interaction with hydrocarbons

There are numerous researches that have focused on the adsorption and interactions of hydrocarbons (HC) on metal oxides since majority of the catalytic reactions are associated with hydrocarbons. Adsorption and interactions of hydrocarbons on ceria and CeO₂ containing compounds are much significant in catalytic processes and automobile emission control systems. Thus the following

section describes adsorption techniques of light hydrocarbons (specially CH_4) over CeO_2 .

Here Figure 2.6 shows how methane gets adsorbed on 2 distinct active sites of ceria. Here the activation process of methane happens through a surface-active oxygen species. The figure shows that surface lattice oxygen anion and surface unsaturated (cus) oxygen are the two species responsible in adsorption of methane on ceria. Here the latter specie can be formed through outgassing at higher temperatures. The cus oxygen has a high electron affinity which tends to have a strong interaction with methane and other light hydrocarbons. At lower temperatures this strong interaction leads in the activation of C-H bond with formation of formates. Then these get decomposed to surface carbonates and finally gets desorbed as CO_2 , and H_2O at comparatively high temperatures (Jin, T. Okuhara T., 1987). Further the literature reveals that once ceria is treated in a reducing environment, the adsorption of methane gets inhibited due to the shortage of cus oxygen and surface oxygen species (Hickey et al., 2001).

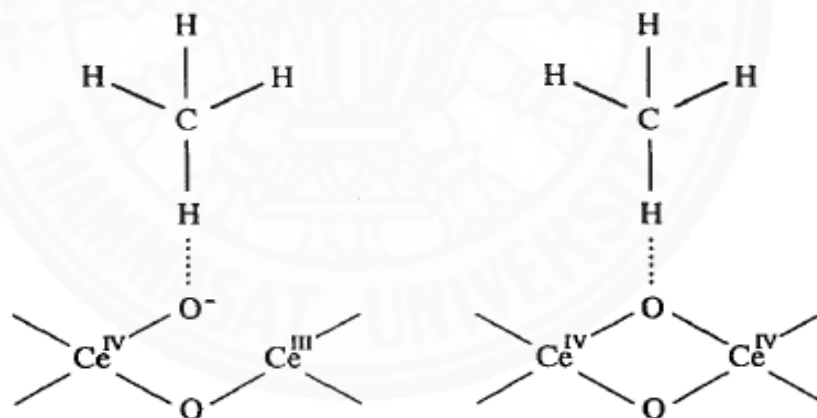


Figure 2.6 Methane adsorbed on two different sites of ceria (Trovarelli, 1996).

Further acid-base sites also play a vital role in determining the extent of adsorption and interaction of hydrocarbons on ceria surface. And also at high temperatures, it is better to have strong acid sites on surface of ceria for better activation of hydrocarbons. Once acid-base pair is strong enough, it is capable of breaking the C-H bond, and give rise to CH_3^- and H^+ ions. Then these two ions have the high possibility

of interacting with the acid and base sites respectively (Duprez, Descorme, Birchem, & Rohart, 2001).

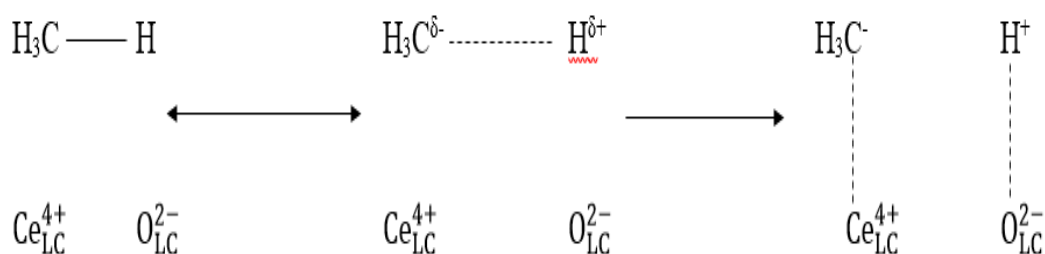


Figure 2.7 Adsorption of HC on acid-base sites of CeO₂ (Trovarelli, 1996).

2.5.3 CeO₂-doped Al₂O₃ support

Based on above unique properties of γ -Al₂O₃ support and CeO₂ supports, conventional Al₂O₃ support can be modified through partial doping of Ce into Al₂O₃ framework, which might give a much better active support to be used for low temperature methanol steam reforming reactions. And following describes some of the techniques that will be used for characterization evaluation of the modified support in this study.

2.5.3.1 Viscosity tests

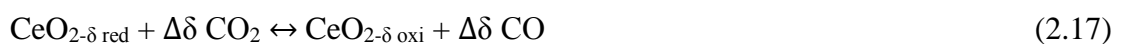
The literature says that application of magnetic inducement affect to have an increment in viscosity of aqueous solutions, so this phenomenon can be analyzed by applying a magnetic field during sol gel preparation of the CeO₂ doped Al₂O₃ support (Han, Guo, & Chai, 2012). Generally, around pH 6 the Ce-Al solution starts its gelation so a temporary magnetic field can be applied to the Ce-Al solution separately at pH 6, 7, 8 and 9 and measure the viscosity. This should be done for N-N, N-S and no magnetic field arrangements. This experiment should be carried out during a time period when there are no much fluctuations in the temperature. Thus this data can be used to analyze to see whether magnetic inducement effects to have a change in the viscosity of the Ce-Al gel during support preparation and cause a hindrance for the motion of ions.

2.5.3.2 Thermogravimetric analysis (TGA)

Normally CeO₂ is a component which is intensely incorporated as a catalyst support because of its unique redox characteristic of being able to have an effective oxygen storage and release. This property which is commonly known as “Oxygen Storage Capacity” or “Oxygen exchange capacity” (OEC, $\Delta\delta$) can be quantitatively evaluated using different analysis methods such as chemisorption, Temperature programmed reduction and desorption and thermogravimetry technique (P. Li, Chen, Li, & Schwank, 2019).

Several research papers claim that the Thermogravimetric analysis (TGA) of the ceria samples can be conducted using Al₂O₃ crucibles. The samples are well cleaned using oxygen gas and argon gas at 200 °C. Then sample is oxidized upto 1000 °C with argon gas flow with a heating rate of 20 °C/min. Then sample is kept at isothermal stage at 1000°C for about 1 hour. Then sample is reduced at 800°C with air zero flow with a cooling rate of 10°C/min and kept isothermally at 800°C for 70 minutes. These oxidation and reduction cycles are repeated twice. Thus according literature, the OEC ($\Delta\delta$) is calculated using the relative difference of weight of the steady-state sample at its reduction and re-oxidation in the second redox cycle (Laosiripojana & Assabumrungrat, 2008). This is to test whether there is a difference in Oxygen Exchange Capacity of each support depending on the magnetic pole arrangement they were prepared and the amount of Ce doped into the γ - Al₂O₃ framework.

Here, in first step, ceria is reduced to get oxygen vacancies at high temperature and low partial pressure. Then these oxygen vacancies are consumed in a second step such that, ceria is subjected to exothermal oxidation. Here it provides CO by abstracting oxygen from CO₂ or yield H₂ from H₂O. Thus the difference between the thermochemical stable oxygen of the redox material at oxidizing conditions (δ_{oxi}) and reducing conditions (δ_{red}) can be counted as the oxygen exchange capacity. (OEC, $\Delta\delta = \delta_{\text{red}} - \delta_{\text{oxi}}$)



2.5.3.3 Hydrogen temperature programmed reduction (H₂-TPR)

According to the previous literature H₂-TPR technique can be used to analyze CeO₂-doped Al₂O₃ supports. Thus Temperature programmed reduction profiles of supports with different CeO₂ loadings and different magnetic pole arrangements during preparation methods can be used to analyze the strength of interaction of Ce with Al₂O₃ framework. This can be done by analyzing the shift of peak temperatures and the hydrogen consumption of each peak of each tested support. The experiment can be carried out by preheating each support with a stream of He gas for 1 hour at 423K. And the after allowing it to come to room temperature pass a flow of 10% H₂/Ar (30 ml/min) at a rate of 10 K/min upto 1373K while the TCD signal is recorded (Damyanova, Perez, Schmal, & Bueno, 2002). For these experiments to be carried out Chemisorption catalyst analyzer (BELCAT-II, BEL Japan Inc., Japan) can be used.

2.6 Oxygen Vacancy

An oxygen vacancy is a defective site in a support framework at the point where the oxygen atom is missing. These sites are formed when the number of oxygen atoms in the crystal lattice is less than the perfect lattice. Here one oxygen atom requires two electrons to make an octet in perfect crystal lattice. Therefore, each oxygen vacancy site is with two trapped electrons ready for a reaction or bonding with active metal atoms or any adsorbed species. Active metal atoms tend to bind on these oxygen vacancy sites due to electron localization effect. The charge transfer to the active metal increases their electron density (Pintado, 2004).

The role of oxygen vacancies towards the adsorption properties was investigated by several studies (Riedo et al., 2001). The Literature reported that the Pd atoms are preferred to adsorbed on oxygen vacancy sites of MgO. The CO adsorption on the Pd active sites was also investigated, in terms of bond length and binding energy Here, the Pd atoms bonding to the surface at oxygen vacancy sites shows a stronger interaction from its larger binding energy and shorter bond length (3.42 eV and 1.524 Å, respectively), compared to bonding at regular MgO sites (0.96 eV and 2.210 Å, respectively).

The defective surfaces of the support from oxygen vacancies normally function as nucleation centers for the growth of active metal clusters, yet they can develop the

properties of deposited cluster or adsorb species through electronic interaction (Bedrane, Descorme, & Duprez, 2002). Considering only the oxide support surface, the surface with oxygen vacancies is also more reactive compared to perfect oxide. Therefore, these defective surfaces can stabilize supported clusters, prevent agglomeration of metal particles and provide an easier adsorption and dissociation of the adsorbed species.

2.7 Catalyst preparation methods

Catalyst preparation methods should be highly examined and concerned when it is required to improve the activity and selectivity of catalysts. The most common technique is called wetness impregnation. This method is very popular because of being simple and time efficient. Wetness impregnation is done by pouring solution of active metals onto the support material in a container and the metals are set to be absorbed into the pores of the support naturally. However, its drawbacks are low driving force which impairs the metal distribution through pores, and it may tend to have agglomerations of active metals on the support surface. Thus, sol-gel method can be incorporated as an alternative to improve the distribution of active metals (Volovych, 2014).

In sol-gel catalyst preparation method the initial metal-support sample is in liquid-phase. And then progressively metallic particles get solidified such that they get stored into the network structure of the support in gel form. The significant benefits of sol-gel technique are that the finally prepared catalyst is with high purity, homogeneity, and moderate porosity. Further it has the ability to provide the final catalyst with large surface area at low temperature (Esposito, 2019). The parameters that should be taken into extra consideration during the catalyst preparation process using sol-gel technique are temperature of gelation, amount of active metal, the final pH of the catalyst, and pretreatment methods. Further metal particle size also affects for the distribution and in this method there is a less possibility of active metals subjecting to sintering or agglomeration. Therefore, this formation of network would provide a strong driving force towards metals to be dispersed into the pores of the support, as well as prolonging the retention time for the magnetic inducement to take place (Cauqui, 1992).

2.8 Effect of magnetic field towards ions

Usually sol-gel method is used to prepare the doped supports with a low amount of dopants since it enhances the dopant distribution throughout the support framework. Thus the final properties of the doped support prepared using this technique basically depend on various preparation parameters, such as, the properties of ions and solution themselves, gelation time, viscosity and pH adjustment. In this study, the effect of magnetic field inducement in different magnet orientations are studied towards the final properties of CeO₂ doped Al₂O₃ support and Cu-Zn based catalysts.

The extent of distribution of doped Ce in Al₂O₃ framework could be one of the factors to alter the properties of support, which could be controlled by the magnetic inducement during sol-gel preparation. Therefore, in this section, literatures related to the effects of magnetic inducement towards ions and solution properties will be broadly discussed.

Magnetic fields have the ability of controlling various chemical and physical phenomena. It generates a force to be acted on a charged particle to alter its motion pattern. The force acting is represented by the following equation.

$$F_B = |q|vB\sin(\phi) \quad (2.16)$$

Where

- q is a charge of the particle
- v is the velocity of the moving particle
- B is magnetic field
- ϕ is the angle between the directions of velocity and magnetic field

Above equation clearly shows that the magnitude of magnetic force applied on the charge particles in magnetic field is directly proportional to the charge (q) and velocity (v) of the particle, also the intensity of the magnetic field (B). The magnetic force also depends on the angle between magnetic field and velocity direction, the maximum force can be obtained when that two parameter are perpendicular between each other. The pathway of positive charge particle moving in magnetic field can be described through following figures (Franczak, Binnemans, & Fransaeer, 2016).

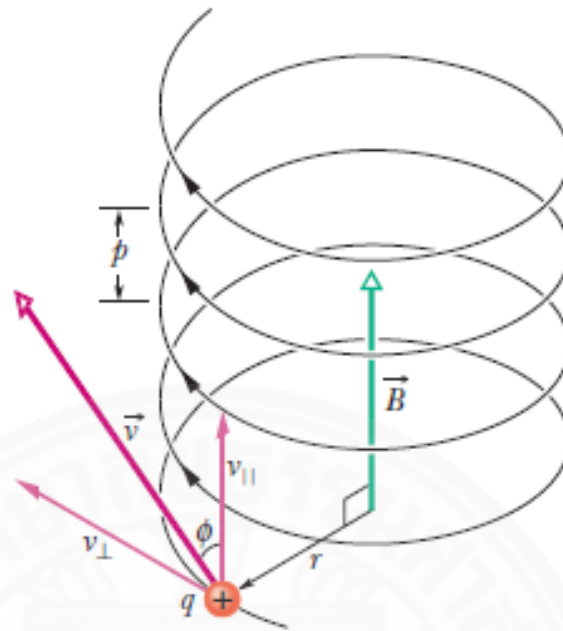


Figure 2.8 A charged particle having a velocity vector that has a component parallel to a uniform magnetic field moves in a helical path (Halliday et al., 2013).

There are literature records which study about the motion of diamagnetic microparticles in a weak magnetic field under ferrofluid (Fujiwara, Mitsuda, & Tanimoto, 2006). The apparatus consists of diamagnetic particles in a ferrofluid core stream at the center, sandwiched by two diamagnetic stream which is the mixture of water and glycerol. The apparatus was placed in a uniform magnetic field. They found that diamagnetic particles move to the opposite direction of the magnetic field and move towards the diamagnetic streams. The diamagnetic particles migrate away from the magnetic source. The effect of magnetic field strength, fluid flow rate, and concentration were also studied. The stronger magnetic field leads to a stronger migration of both magnetic nanoparticles and diamagnetic nanoparticles. The higher fluid flow rate causes a higher concentration gradient of both particle types. Lastly, the higher concentration of diamagnetic ions in the system leads to a stronger interaction between particles resulting in a weaker migration (less particles spread out in the system) (Zhu, Hejiazan, Huang, & Nguyen, 2014).

Further, literature claims that the application of an external inhomogeneous magnetic field is capable of providing an extra inducement for the movement of

molecules and ions in solution. The magnitude of the magnetic force applied on species in a magnetic field can be determined through magnetic character of each metal ions. Magnetic property of metal ions might be either paramagnetic or diamagnetic. Paramagnetic species normally have unpaired electrons in their atomic orbitals (TADA, 2011). Literature reveals that electrons possess spins which can be counted as permanent magnetic dipole moments. When there is no external magnetic inducement, the magnetic dipole moments of paramagnetic ions lead to have random orientations such that they get cancelled each other (Rodrigues et al., 2017). But when subjected to an external magnetic inducement, the magnetic dipole moments of the paramagnetic species get aligned with the line of magnetic flux (Rikken et al., 2014).

In contrast, diamagnetic species have no unpaired electrons in atomic orbitals where they do not get subjected in magnetization (TADA, 2011). Despite all these facts, still an external magnetic field is capable of causing small distortions of the electron orbits with molecules. Here magnetic dipole moments can be induced and made to align in a direction opposite to the magnetic field flux lines. Thus diamagnetic species can have dipole magnetic moments under the influence of external magnetic field and magnetic moments will remain in the samples as long as the magnetic field is applied (Kolczyk et al., 2016).

Thus in summing up all these details, it can be clearly described that once a magnetic field with a gradient is applied paramagnetic metal ions have a tendency to move in the direction of increasing magnetic field, where as the diamagnetic metal ions move away from the stronger magnetic field (Franczak et al., 2016).

This knowledge about magnetic inducement towards ions movement and solution properties can be further applied to the development of Cu-Zn catalyst in MSR. With the different charge and size of Ce^{4+} and Al^{3+} , they can move differently in a magnetic field induced aqueous solution which could enhance mixing of Ce and Al during support preparation by sol-gel method. The increasing in the degree of Ce-doped in Al_2O_3 framework can affect interaction of an active metal to the support and the catalytic activity of Hydrogen production. The effect of magnetic field inducement toward the activities of Cu-Zn catalysts will also be investigated in this study.

CHAPTER 3

METHODOLOGY

3.1 Chemicals and materials

Here the catalyst modification is done by two distinct approaches. The first task is the application of magnetic inducement with different magnetic pole arrangements during the sol-gel preparation of the CeO₂-doped Al₂O₃ support. While the second goal is the application of magnetic inducement during the sol-gel process of Cu-Zn metal loading into the supports prepared in accordance to the first task. All the chemicals involved in this research are listed in Table 3.1

Table 3.1 List of chemicals used in experiments.

Chemicals	Concentration	Company	Purpose
Ce(NO ₃) ₃ ·6H ₂ O	≥97%	Acros organics	Doped support preparation
Al(NO ₃) ₃ ·9H ₂ O	≥97%	Fluka Chemical Corp.	
Ammonia solution	30 vol%	Loba Chemie	
γ-Al ₂ O ₃	≥99%	Sigma-Aldrich	reference support
α-Al ₂ O ₃	≥99%		
Quartz powder 200μm		Sigma-Aldrich	
Cu(NO ₃) ₂ ·3H ₂ O	≥97%	Sigma-Aldrich	Cu-Zn catalyst preparation
Zn(NO ₃) ₂ ·6H ₂ O	≥97%		
C ₆ H ₈ O ₇ ·6H ₂ O	≥97%	Merck	
Methanol	≥99%	Loba Chemie	MSR reaction

3.2 Catalyst preparation

3.2.1 Preparation of CeO₂-doped Al₂O₃ support

The CeO₂-doped Al₂O₃ supports were prepared under different magnetic field environments. Nine rectangular neodymium magnets with the size of 40 mm × 30 mm × 12.5 mm and surface magnetic field of 320 mT are attached to a metal plate in 3×3 configuration. These metal plates were attached to the aluminum frame which was prepared to be the magnet holder.

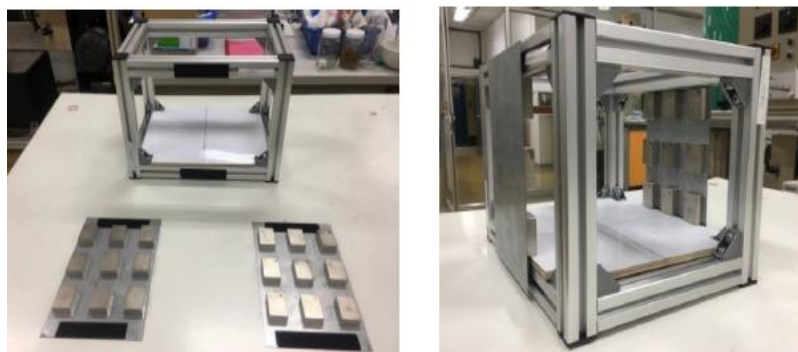


Figure 3.1 Magnetic device component and set up.

CeO₂-doped Al₂O₃ supports were prepared with 5mol% of CeO₂ in Al₂O₃ using a sol-gel method. Ce(NO₃)₃·6H₂O and Al(NO₃)₃·9H₂O were separately dissolved in deionized water to form 0.5 M salt solutions. The prepared 0.5 M Ce salt solution was mixed with the Al salt solution to form Ce-Al salt solutions with a 0.05:0.95 molar ratio. The Ce-Al salt solutions were placed in environment with different magnetic arrangements; No magnet, North-South pole (N-S), and North-North pole (N-N). An ammonia solution was slowly dropped into the mixed salt solutions to form a gel until the pH value reached 9 within 90 minutes. The prepared gels corresponding to the three magnetic arrangements were kept at room temperature for 48 h, dried at 110 °C for 24 h, calcined at 800 °C for 4 h to obtain CeO₂-doped Al₂O₃ supports. All supports were grinded and sieved at 106 μm to control the size of support particles.

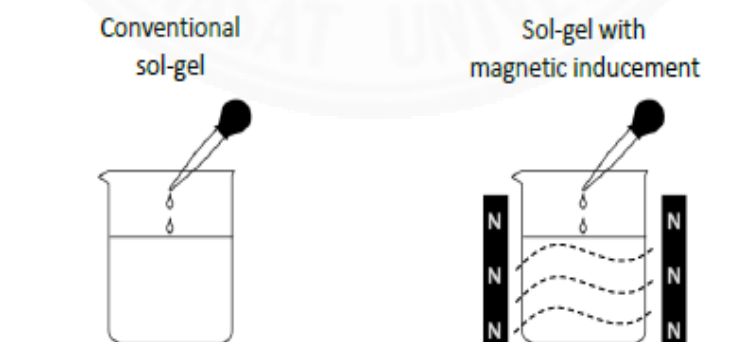


Figure 3.2 Schematic of magnetic device for sol-gel support preparation.

3.2.2 Preparation of Cu-Zn/CeO₂-doped Al₂O₃ catalyst

5wt% Cu-Zn/5mol% CeO₂-doped Al₂O₃ and 5wt% Cu-Zn/ γ -Al₂O₃ were prepared by sol-gel method with magnetic inducement. Copper nitrate trihydrate (Cu(NO₃)₂·3H₂O, Sigma-Aldrich), zinc nitrate hexahydrate (Zn(NO₃)₂·6H₂O, Sigma-Aldrich) and citric acid monohydrate (C₆H₈O₇·6H₂O, Merck) were dissolved in DI water to form Cu-Zn metal solution before being poured into CeO₂-doped Al₂O₃ support(prepared in accordance to the above method) and γ -Al₂O₃ support respectively. Then pH was adjusted by stirring and adding ammonia solution drop by drop until it reached 7. Then the sol-gel sample is kept within a magnetic field for drying at room temperature until the sol-gel samples become dried. The magnetic pole arrangements are N-N, N-S and no magnetic field. These samples were dried at 110 °C overnight, then calcined at 300 °C for 3 h. After that, calcined catalysts were grounded into fine powder.

3.2.3 Preparation of Cu-Zn/ α -Al₂O₃ catalyst

Cu-Zn/ α -Al₂O₃ catalysts were prepared with the prominent objective of understanding the motion pattern of Cu ions and Zn ions in semi liquid media under the magnetic field inducement. Less porosity of α -Al₂O₃ support compared to γ -Al₂O₃ support was the major reason to prepare Cu-Zn/ α -Al₂O₃ catalysts, where it ensures the surface motion of Cu ions and Zn ions under magnetic field.

8 cm x 9 cm homogeneous and flat α -Al₂O₃ plate was prepared by 6 g of α -Al₂O₃ powder and 5 ml of DI water. The experiment was carried out separately to prepare 3 distinct catalysts Cu/ α -Al₂O₃, Zn/ α -Al₂O₃, and Cu-Zn/ α -Al₂O₃. Here a drop of 1 ppm of Cu²⁺ aqueous solution, Zn²⁺ aqueous solution Cu²⁺-Zn²⁺ were put to the center of the α -Al₂O₃ plates respectively. These prepared catalysts were kept at 2 different magnetic pole arrangements N-N and N-S and no magnetic field for 2 hours at room temperature allowing the motion of ions with no external disturbance like stirring. Then from each catalyst 6 equally sized slices were taken out as 2 pieces each respectively very much closer to the 2 magnets (B1, B2, C1, C2) and the other 2 (A1, A2) surrounding the center of the α -Al₂O₃ plate where the initial drop was put. The dimension of each strip is 1mm x 2mm. Following is a rough diagram of the geometrical dimensions of the α -Al₂O₃ plate and how the 2 magnets are placed. Then each catalyst

sample was microwave digested with suitable temperatures and solvents to remove carbon traces and make the solid samples a homogeneous solution. Then each sample was analyzed through atomic absorption spectroscopy to get the corresponding concentration of each ion in each catalyst slice.

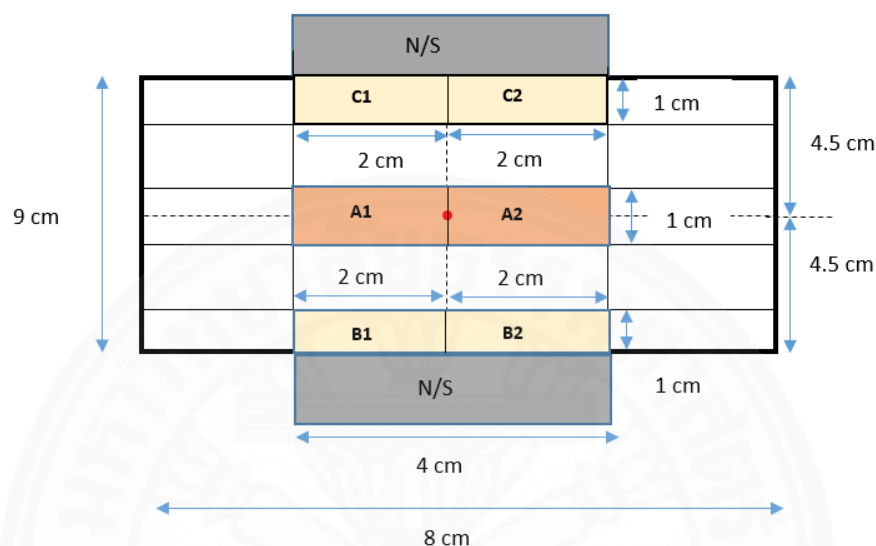


Figure 3.3 Geometrical image of alpha alumina powder plate.

3.2.3.1 Microwave digestion method for Cu/ α -Al₂O₃ catalysts

The 6 catalyst pieces (A1, A2, B1, B2, C1, C2) of (1 mm x 2 mm) dimensions taken out from the α -Al₂O₃ catalysts plate were dried at 60 °C for 7 minutes and grinded well to be in fine powder form. The dried weight of each catalyst was around 0.4–0.45 g. Then each catalyst was microwave digested with 10 ml of 70 vol% HNO₃ acid. The heat energy was supplied such that all the Cu²⁺ ions attached in the alumina framework gets well dissolved. First the catalyst samples were heated upto 160 °C with a ramping rate of 25 K/min and kept isothermally at 160 °C for about 5 minutes. Then in the second stage temperature was increased upto 190 °C with a ramping rate of 10 K/min and held isothermally at 190 °C for about 20 minutes. Then finally the catalyst samples were cooled down to 50 °C within 140 minutes and held at 50 °C for 15 minutes. Then the acid digested samples were filtered using No 1 filter paper following a dilution upto 100 ml. Then before analyzing under AAS each diluted sample was filtered from a 0.25 μ m PTFE syringe filter since the particle size in the final solution should be less than 10 μ m.

3.2.3.2 Microwave digestion method for Zn/ α -Al₂O₃ catalysts

Here also the 6 catalyst pieces (A1, A2, B1, B2, C1, C2) of (1 mm x 2 mm) dimensions taken out from the α -Al₂O₃ catalysts plate were dried at 60 °C for 7 minutes and grinded well to be in fine powder form. The dried weight of each catalyst was around 0.4–0.45 g. Then each catalyst was microwave digested with 10 ml of 70 vol% HNO₃ acid. The heat energy was supplied such that all the Zn²⁺ ions attached in the alumina framework gets well dissolved. First the catalyst samples were heated upto 170 °C with a ramping rate of 25 K/min and kept isothermally at 170 °C for about 5 minutes. Then in the second stage temperature was increased upto 210 °C with a ramping rate of 12 K/min and held isothermally at 210 °C for about 40 minutes. Then finally the catalyst samples were cooled down to 50 °C within 160 minutes and held at 50 °C for 20 minutes. Then the acid digested samples were filtered using No 1 filter paper following a dilution upto 100 ml. Then before analyzing under AAS each diluted sample was filtered from a 0.25 μ m PTFE filter since the particle size should be less than 10 μ m.

3.2.3.3 Microwave digestion method for Cu-Zn/ α -Al₂O₃ catalysts

Since these catalyst samples contain both Cu⁺ and Zn²⁺ ions attached in alumina framework, the acid digestion should be carried out such that both the ions get well dissolved. So for these catalyst samples the acid digestion method described in 3.2.3.2 section was applied. (The method carried for acid digestion of Zn²⁺ ions).

3.3. Methanol steam reforming reaction

3.3.1 Catalytic activity test

The MSR was studied on the prepared catalysts in a quartz tubular reactor. On each experiment, 0.1 g of catalyst was mixed with 0.4 g of quartz sand in order to provide better temperature distribution and then packed between quartz wool. The catalyst was reduced with 50 vol% of H₂ in Ar at 300 °C for 1 h before MSR reaction. Then, the reactor was flushed with 20 mL/min Ar to purge the left over H₂. 20 mL/min of Ar were flowed into each saturator containing water at 100 °C, and methanol at 65 °C to obtain a mixture of 1:1 methanol-to-water molar ratio. The reactions were

performed at 200, 225, 250, 275 and 300 °C in a continuous mode. The produced gas was sent to an auto-sampling unit and analyzed by gas chromatography coupled with a thermal conductivity detector (GCMS-2010 Ultra, Shimadzu Corporation, Japan) to determine the amount of hydrogen production.

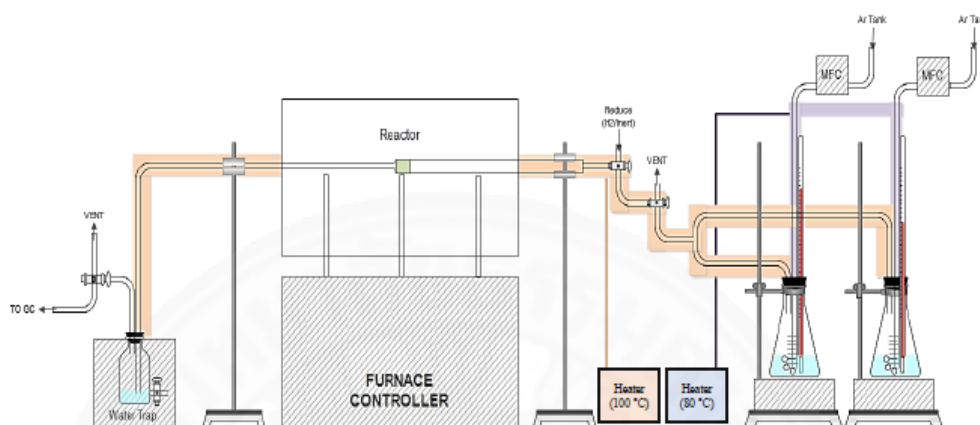


Figure 3.4 Schematic of lab scale methanol steam reforming process.

3.4 Characterization

3.4.1 Support characterization

3.4.1.1 BET analyzer

The BET technique by physical adsorption of N_2 was evaluated on different supports in order to determine characteristics such as specific surface area, pore volume, and pore diameter of CeO_2 -doped Al_2O_3 support compared to $\gamma-Al_2O_3$ (Autosorp-1, Quantachrome, USA). The support was packed in the sample tube, then equipped in the instrument. The blank sample tube is also installed to the instrument to be used as a reference. Prior to the measurement, degassing process is required to make an empty surface. The sample was heated to 300 °C under vacuum atmosphere for 12 h, cooled down to a room temperature under He inert flow. After that, both tubes were vacuumed again to get rid of all the gases and immersed on the liquid nitrogen. N_2 gas was introduced into both tubes and a difference in pressure was measured in terms of P for sample tube and P_0 for reference tube. The N_2 adsorption data were calculated by using Brunauer-Emmett-and-Teller (BET) equation to determine the surface area, pore volume, and pore diameter.



Figure 3.5 BET analyzer (N₂ physical adsorption instrument).

3.4.1.2 X – ray Diffraction (XRD)



Figure 3.6 X - ray diffraction instrument.

The X-ray diffraction technique (XRD, X'Pert PRO diffractometer, Panalytical, Almelo, the Netherlands) using Cu K α_1 radiation at 40 kV and 45 mA, (20°–90°) 2-theta, 0.02° step size, 0.2 sec step time was used to determine the crystal structure properties of the supports. The XRD patterns of the supports were undergone peak

deconvolution prior to determination of the lattice constant. The lattice constant of Al_2O_3 in different supports were calculated using the highest diffraction plane (4 0 0) and (4 4 0), which corresponds to the diffraction angle of 46 and 67 degrees, respectively.

3.4.1.3 Scanning electron microscopy with energy dispersive spectroscopy (SEM-EDS)

Ce composition and distribution in the Al_2O_3 framework were determined by a Field Emission Scanning Electron Microscope (FE-SEM, HITACHI, SU-5000) coupled with the Energy Dispersive Spectrometry (EDS, Horiba) operated in point elemental analysis. The sample was magnified approximately at 20,000x, energy range of 20 keV, and accelerating voltage of 15 kV. Ce composition and distribution of each supports were evaluated randomly from 5 points each on 5 different particles of each support. The average values and standard deviation of the Ce:Al molar ratio were calculated to illustrate the dispersion of Ce in Al_2O_3 framework prepared by different magnetic inducement environment.

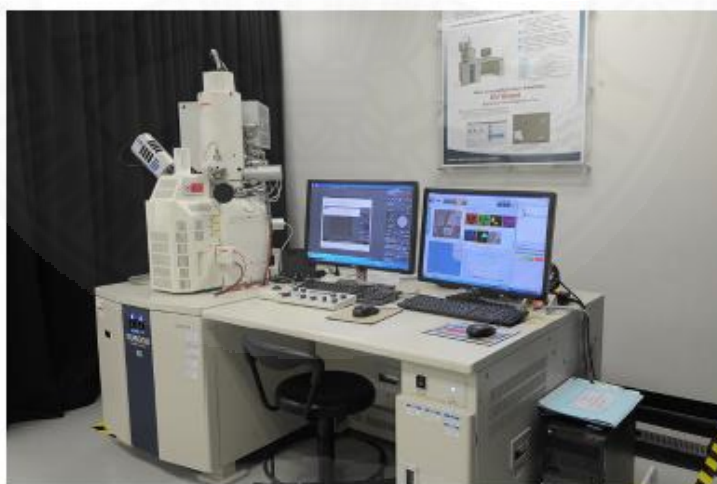


Figure 3.7 Scanning Electron Microscopy with Energy Dispersive Spectroscopy.

3.4.1.4 X-ray Photoelectron Spectroscopy (XPS)

X-ray photoelectron spectroscopy analysis (XPS) is done using a Kratos Axis Supra XPS spectrometer incorporated with a monochromated $\text{Al K}\alpha$ x-ray source which are operated at 15 mA and 15 kV. This technique was used in determination of XPS

spectra for CeO₂-doped Al₂O₃ supports prepared with and without magnetic inducements. The XPS peak pattern of each support was analyzed to determine the oxidation state of Ce in the differently prepared supports.

3.4.2 Catalyst characterization

3.4.2.1 Atomic Absorption Spectroscopy (AAS)

The Atomic Absorption Spectroscopy was used to analyze the concentrations of Cu²⁺ ions and Zn²⁺ ions separately on α -Al₂O₃ support. The catalyst samples were acid digested as explained earlier to remove carbon traces. Then the samples were 1 time diluted such that the concentrations of ions lie within the detectable region. The maximum Cu²⁺ concentration readable through the equipment is 1.6 ppm while for Zn²⁺ the maximum readable concentration is 0.75 ppm. The diluted catalyst samples were filtered through 0.25 μ m PTFE filter since the size of the particles in the samples should be less than 10 μ m.

CHAPTER 4

RESULTS AND DISCUSSION

The catalytic activity of the common Cu-Zn based catalyst for MSR can be improved by applying magnetic inducement to the conventional sol-gel catalyst preparation method. Thus here the two approaches of using magnetic inducement for catalyst improvement are 1) for the preparation of CeO₂-doped Al₂O₃ support 2) for the deposition and distribution of Cu and Zn active metals on the so-called prepared support. Thus this chapter elaborates on how the magnetic inducement affects these two approaches in increasing the activity of the Cu-Zn catalyst.

4.1 Effect of magnetic inducement on preparation of 5mol% CeO₂-doped Al₂O₃ support

Here three basic types of supports were prepared by applying N-N and N-S magnetic pole arrangements and one reference support with no magnetic field during their sol-gel preparation. The prepared three supports are –

- 1) 5mol% CeO₂-doped Al₂O₃ (no magnet)
- 2) 5mol% CeO₂-doped Al₂O₃ (N-N)
- 3) 5mol% CeO₂-doped Al₂O₃ (N-S)

These three supports were then used to prepare the 5wt% Cu-Zn catalyst where no magnetic field was applied during the metal loading. Thus below mentioned are the three catalysts prepared finally –

- 1) 5wt% Cu-Zn (no magnet)/5mol% CeO₂-doped Al₂O₃ (no magnet)
- 2) 5wt% Cu-Zn (no magnet)/5mol% CeO₂-doped Al₂O₃ (N-N)
- 3) 5wt% Cu-Zn (no magnet)/5mol% CeO₂-doped Al₂O₃ (N-S)

Thus the following sections describe the amount of hydrogen yield by each catalyst through MSR and characterization of three supports.

4.1.1 Hydrogen Production rates obtained through MSR

The above mentioned three catalysts were tested for methanol steam reforming reaction for five different temperatures 200, 225, 250, 275 and 300 °C.

Table 4.1 H₂ production rate over 5wt% Cu-Zn catalysts (no magnet) on 5mol% CeO₂-doped Al₂O₃ supports prepared with and without magnetic inducement.

Magnetic inducement and pole arrangement	H ₂ production rate (μmol/min)				
	200 °C	225 °C	250 °C	275 °C	300 °C
No magnet	150±30	371±43	619±61	850±80	1095±92
N-N	175±50	754±60	1349±99	1800±99	2099±99
N-S	167±42	530±40	916±42	1388±72	2002±90

Table 4.1 shows H₂ production rates for Cu-Zn catalysts supported on CeO₂-doped Al₂O₃ prepared with and without magnetic inducement. The effect of using different magnetic inducements during support preparation on the catalytic activity is only observable within the temperature range 225-275 °C. Here the catalyst prepared over (N-N) support yields twice the hydrogen compared to the catalyst prepared over (no magnet) support within 225-275 °C. At 200 °C, the hydrogen yield by all the three catalysts is approximately the same with a slight difference. This slight difference implies that, by that temperature the catalysts have not overcome the activation energy to differentiate the effect of magnetic inducement towards the support preparation. Again at 300 °C, all the three catalysts may have undergone deactivation where again it does not describe the effect of magnetic inducement on supports.

4.1.2 Doping of Ce into Al₂O₃ framework with and without magnetic inducement

To establish the fact of the replacement and/or insertion of dopants into Al₂O₃ framework, the XRD patterns of the CeO₂-doped Al₂O₃ supports with and without magnetic inducement were investigated. All supports have similar XRD patterns which correspond to the standard XRD pattern of γ -Al₂O₃, cubic structure; (2-theta around 46 and 67 degrees). All the supports also show sharp peaks of CeO₂, cubic structure; (2-theta around 28, 33, 47, and 56 degrees). The important characteristic peaks of Al₂O₃ are analyzed to calculate the lattice constant of the support structure.

According to Table 4.2, since the lattice constant of γ -Al₂O₃ and CeO₂-doped Al₂O₃ show different values it can be implied that Ce has been successfully inserted and distributed into the Al₂O₃ framework. The cation vacancies in the defect spinel structure of γ -Al₂O₃ may increase the opportunity to partial dope Ce atoms into Al₂O₃ framework to cause a change or adjustment in unit cell because of the larger atomic

radius of Ce. This eventually provides a higher lattice constant compared to commercial and in-house gamma alumina support.

The highest lattice constant is achieved when the supports were prepared with the same-pole magnetic inducement. It is implied that magnetic inducement with same pole of magnet can enhance the partial doping of Ce into Al_2O_3 framework. But the home made gamma alumina support takes a higher lattice constant value compared to commercial gamma alumina, implying that industrial bulk production may cause less defects in the spinel structure of $\gamma\text{-Al}_2\text{O}_3$. In addition, the lattice constants of CeO_2 -doped Al_2O_3 supports prepared with and without magnetic inducement has only small variations, which manifest that the magnetic inducement during support preparation has less influence on the crystal structure of $\gamma\text{-Al}_2\text{O}_3$.

Table 4.2 Lattice parameters derived from XRD graph.

Support		Lattice constant [Å]
Commercial $\gamma\text{-Al}_2\text{O}_3$		7.8683
In-house $\gamma\text{-Al}_2\text{O}_3$		7.8721
5mol % CeO_2 -doped Al_2O_3	No mag	7.8810
	N-N	7.8962
	N-S	7.8864

Table 4.3 BET surface area data.

Support	Magnetic inducement	Surface area (m^2/g)	Pore volume (cm^3/g)	Average pore diameter (Å)
$\gamma\text{-Al}_2\text{O}_3$	No magnet	175.6	0.29	66.7
CeO_2	No magnet	46.6	0.11	80
5% CeO_2 -doped Al_2O_3	No magnet	138.1	0.33	94.3
	N-N	135.6	0.33	96.3
	N-S	142.2	0.32	91.2
3% CeO_2 -doped Al_2O_3	No magnet	144.6	0.31	88.9
	N-N	141.5	0.32	89.2
	N-S	146.3	0.32	82.2
1% CeO_2 -doped Al_2O_3	No magnet	159.3	0.38	94.4
	N-N	147.6	0.33	93.6
	N-S	152.4	0.32	91.2

Table 4.3 also shows the characteristics of the supports which are studied in this research, comprised of surface area, pore volume, and pore diameter determined by the N_2 physical adsorption (BET technique). The 5mol% CeO_2 -doped Al_2O_3 supports

provide the surface areas within 135.6–142.4 m²/g range. Once the Ce percentage increase the surface area gradually gets decreased. The surface area of CeO₂-doped Al₂O₃ decreases as compared to γ -Al₂O₃ due to larger pore volume and larger average pore diameter. Further, the surface area of supports made with different magnetic pole arrangements do not vary that much for both 5mol% and 3mol% Ce dopants which follow the same pattern as in XRD results.

Depending on the results of table 4.3, it can be clearly observed that the 5mol% CeO₂-doped Al₂O₃ supports under the same pole of magnetic inducement (N-N) have the lowest surface area, which illustrates a high insertion of Ce composition and different Ce distribution in comparable with the other supports. While, the support under different pole of magnetic inducement (N-S) have the highest surface area, which indicates a relatively low insertion of Ce composition in the support framework. Therefore, the magnetic inducement can be used to alter the Ce composition as well as the distribution of Ce into Al₂O₃ framework.

4.1.3 Dispersion of Ce in the Al₂O₃ framework with and without magnetic inducement

The SEM-EDS techniques was used to determine the extent of Ce distribution on the surface of CeO₂-doped Al₂O₃ support by randomly sampling at different points. Here the SEM-EDS data was inconstantly collected from 5 points on 5 particles of each support with the intention of analyzing the Ce composition range and distribution in the Al₂O₃ framework of each support. Following Figure 4.1 elaborates the SEM images of CeO₂-doped Al₂O₃ supports with and without magnetic inducement and indicates the sampling points. Further the Ce composition and distribution are represented in the molar ratio of Ce:Al and the values are listed in Table 4.2.

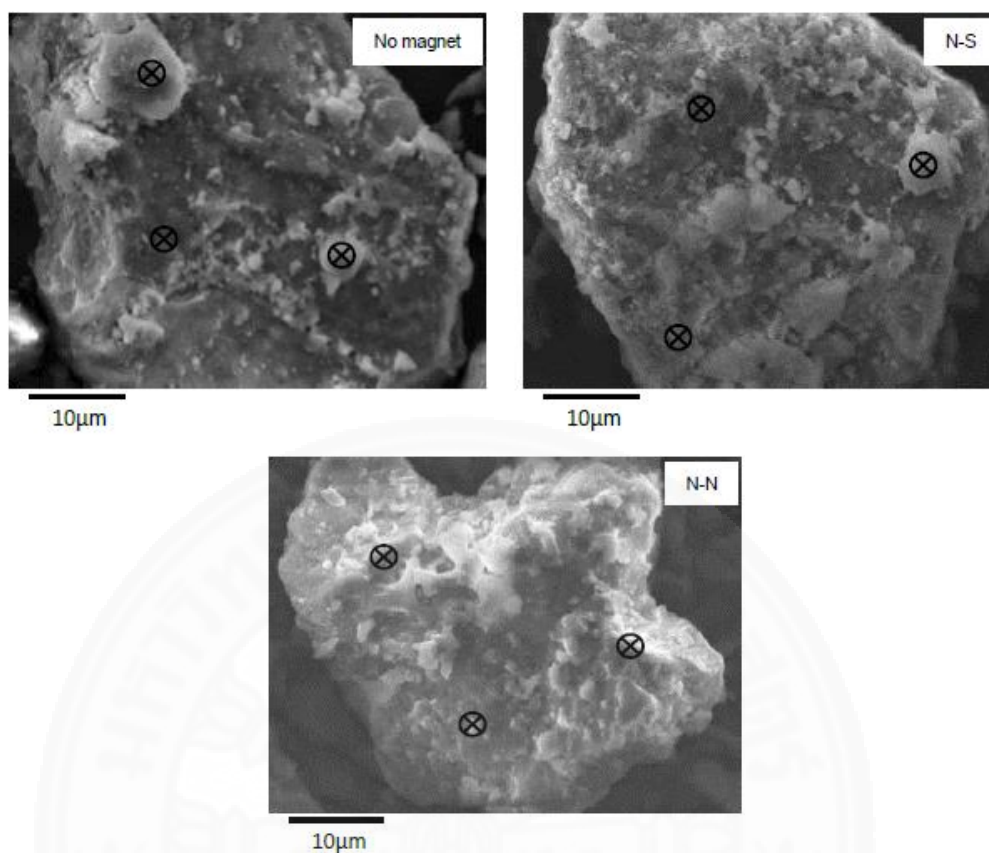


Figure 4.1 SEM images and scanning points of CeO₂-doped Al₂O₃ supports with and without magnetic inducement.

Table 4.4 Ce distribution in CeO₂-doped Al₂O₃ with and without magnetic inducement.

Support	Magnetic inducement	Ce:Al molar ratio x 10 ²		
		Range	Average	SD
CeO ₂ -doped Al ₂ O ₃	No magnet	2.9-14.6	6.9	4.5
	N-N	7.7-8.1	7.8	0.2
	N-S	2.2-2.9	2.6	0.3

The result shows that by applying magnetic field with different pole orientations during support preparation leads to the difference in composition and distribution of Ce. While no magnetic inducement is applied, the range of Ce:Al molar ratio widely varies from 2.9 to 14.6, implying that Ce is randomly inserted in the framework of the support during the sol-gel process. Applying magnetic inducement makes Ce distribution better, which is evident from the narrower range and lower standard deviation of Ce:Al molar ratio. The surface morphology of CeO₂-doped Al₂O₃ are

different between the group with and without magnetic inducement. The one with magnetic inducement show more smooth surface which may show the framework arrangement ability of magnetic inducement.

The result shows that by applying magnetic field with different pole orientations during support preparation leads to the difference in composition and distribution of Ce. While no magnetic inducement is applied, the range of Ce:Al molar ratio widely varies from 2.9 to 14.6, implying that Ce is randomly inserted in the framework of the support during the sol-gel process. Applying magnetic inducement makes Ce distribution better, which is evident from the narrower range and lower standard deviation of Ce:Al molar ratio. The surface morphology of CeO₂-doped Al₂O₃ are different between the group with and without magnetic inducement. The one with magnetic inducement show more smooth surface which may show the framework arrangement ability of magnetic inducement.

The data in Table 4.2 also imply that the magnetic pole arrangement has the ability to affect the Ce composition of different supports. The same pole magnetic arrangement (N-N) obtains a higher Ce composition, in comparison with the different pole magnetic arrangement (N-S). Further, the results clearly match with the results of the surface area of the supports in Table 4.3. The supports prepared with the same pole of magnetic inducement has a low surface area based in its relatively high Ce composition, together with a high uniformity of Ce distribution all over the supports. Thus based on these facts, it can be manifested that the application of magnetic inducement during the sol-gel process can control Ce composition and distribution in CeO₂-doped Al₂O₃ supports. Further the presence of differences in Ce composition and distribution over Al₂O₃ framework may give rise to different catalytic properties.

Further based on the Figure 4.2 the effect of magnetic inducement on Ce composition and distribution over Al₂O₃ framework can be described as follows.

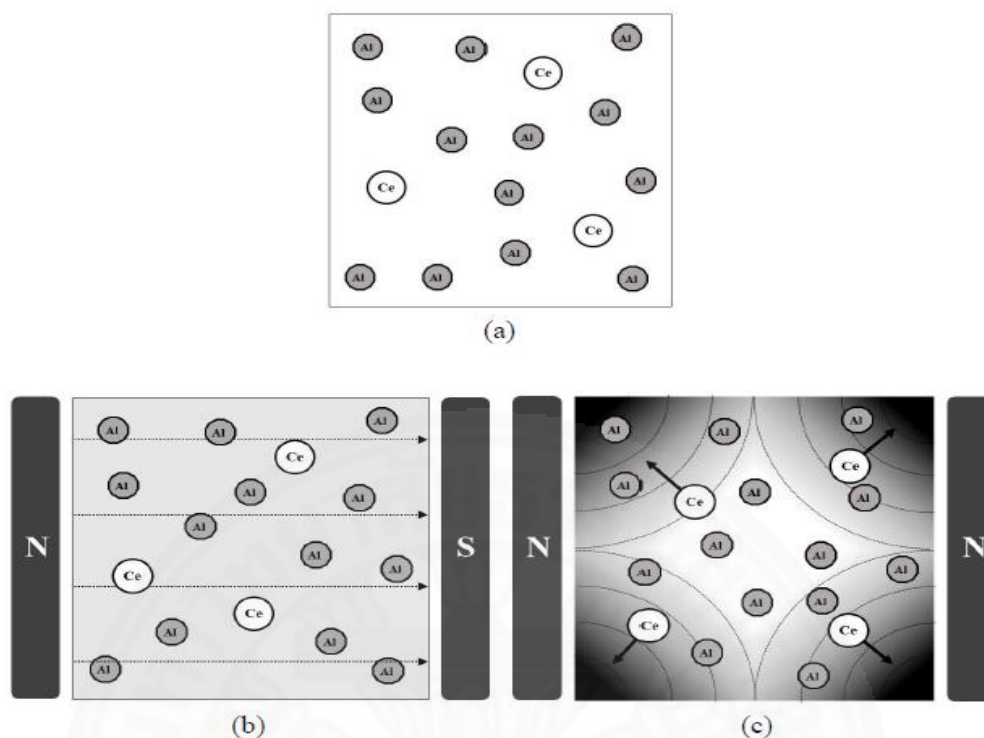


Figure 4.2 Schematics of Ce^{3+} and Al^{3+} movement under (a) no magnetic inducement (b) magnetic field from opposite magnetic field arrangement (N-S) and (c) same magnetic pole arrangement (N-N) (Vacharapong et al., 2019).

In CeO_2 -doped Al_2O_3 supports prepared with no magnetic field, the motion of Ce^{3+} and Al^{3+} ions during gelation process are basically due to homogeneous diffusion; where, both the ions get randomly diffused, having concentration gradient as the one and only driving force.

The support prepared with opposite pole magnetic inducement (N-S) experiences a uniform magnetic field from North pole to South pole, with no effective magnetic field gradient. Thus there is no extra driving force applied to have a special motion of Ce^{3+} and Al^{3+} ions, other than the motion due to random diffusion.

On the other hand, supports prepared under magnetic inducement with same pole arrangement (N-N) provide inhomogeneous scattering magnetic field gradient pattern. Here the magnetic field gradient is able to induce the motion of paramagnetic Ce^{3+} ions towards stronger magnetic field region. Meanwhile diamagnetic Al^{3+} experiences little effect on its movement, causing Al^{3+} to be immobilized while Ce^{3+} ions can penetrate into Al_2O_3 framework (Vacharapong et al., 2019).

In an attempt to determine the oxidation states of Al and Ce, the Al_2O_3 and CeO_2 -doped Al_2O_3 supports were also analyzed with XPS spectrometry. The XPS spectrum of Al 2p and Ce 3d is presented in Figure 4.3 and Figure 4.4, respectively with the list of characteristic peaks presented in Table 4.5.

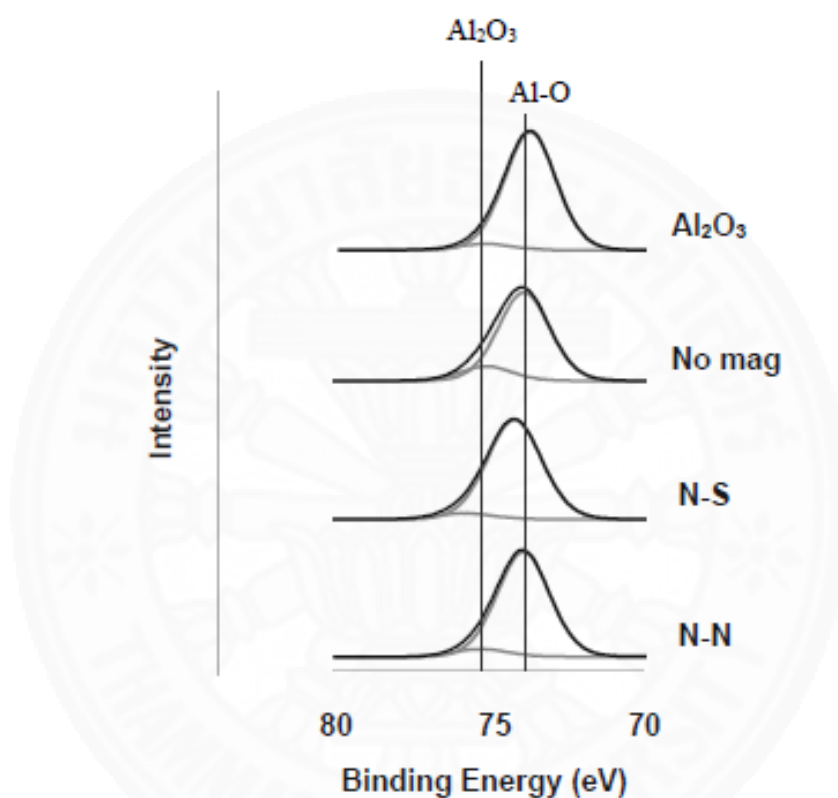


Figure 4.3 Al 2p XPS spectrograms of Al_2O_3 and CeO_2 -doped Al_2O_3 prepared with and without magnetic inducements (Vacharapong et al., 2019).

In Figure 4.3, no significant difference is observed in Al 2p binding energy between Al_2O_3 and CeO_2 -doped Al_2O_3 supports prepared with and without magnetic inducement. In Figure 4.4 and Table 4.5, also there are no much significant change in Ce 3d peaks energy among all the CeO_2 -doped Al_2O_3 supports.

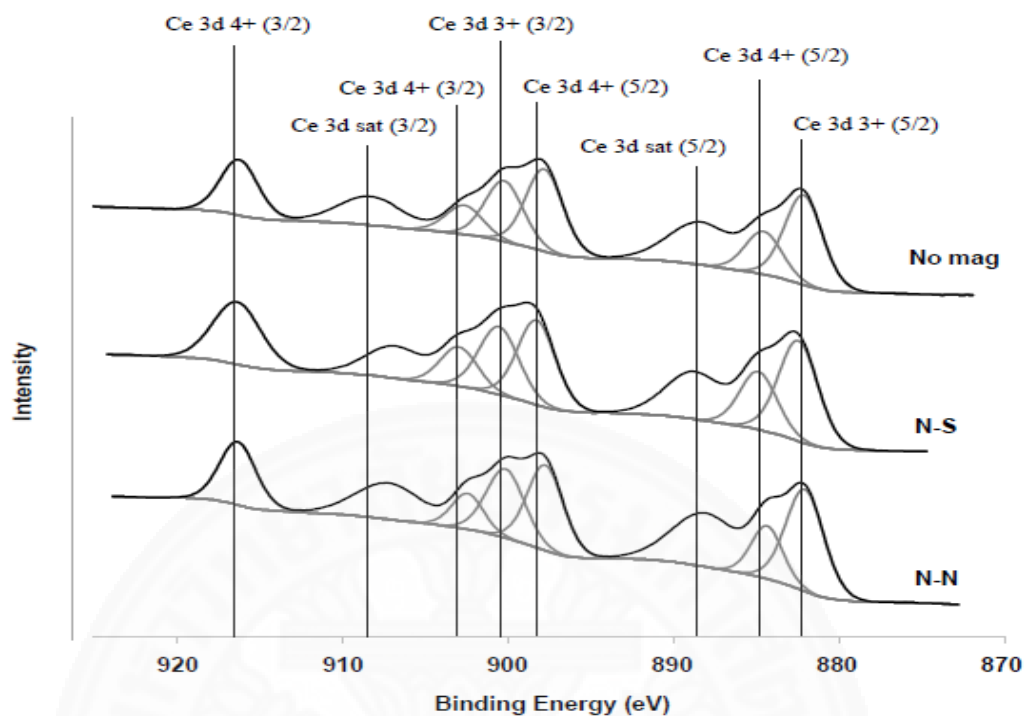


Figure 4.4 Ce 3d XPS spectrograms of CeO₂-doped Al₂O₃ prepared with and without magnetic inducement (Vacharapong et al., 2019).

Table 4.5 Peak energy of Al 2p and Ce 3d XPS spectrograms (Vacharapong et al., 2019) (Vacharapong et al., 2019).

Support	Peak energy (eV)							
	Ce 3d (3+)5/2	Ce 3d (3+)3/2	Ce 3d (4+)5/2	Ce 3d (4+)3/2	Ce 3d (sat)5/2	Ce 3d (sat)3/2		
CeO ₂ doped Al ₂ O ₃	882.12	900.22	884.53	897.79	902.63	916.23	888.36	908.31
CeO ₂ doped Al ₂ O ₃ (N-S)	882.44	900.54	884.85	898.26	902.95	916.36	888.73	906.83
CeO ₂ doped Al ₂ O ₃ (N-N)	882.04	900.14	884.33	897.73	902.43	916.31	888.07	907.20

Therefore, the application of magnetic inducement during CeO₂-doped Al₂O₃ support preparation affects only the Ce distribution and composition in Al₂O₃. The defects based on oxygen vacancy in CeO₂ and the higher composition of Ce in Al₂O₃ framework give rise to have a more homogeneous dispersion of Cu-Zn over CeO₂-doped Al₂O₃ support. Further it suggests that magnetic inducement provide no significant effect on the structure of support. Therefore, the enhanced catalytic activity

of Cu-Zn catalyst over CeO₂-doped Al₂O₃ support prepared under same magnetic pole arrangement (N-N) is mainly because of the relatively higher amount of Cu-Zn active sites formed due to the higher Ce composition in the Al₂O₃ support framework.

4.2 Effect of magnetic inducement on diffusion of Cu²⁺ and Zn²⁺ ions in sol-gel media

To study the diffusion pattern of Cu²⁺ and Zn²⁺ ions under the magnetic inducement in semi liquid state Cu-Zn/ α -Al₂O₃ catalysts were prepared. These catalysts were prepared on a homogeneous flat α -Al₂O₃ powder plate. A drop of 1 ppm Cu²⁺ or Zn²⁺ ions solution was put to the center of the plate and kept at (N-N), (N-S) and no magnetic field arrangements at room temperature. Then just allowed the free motion of ions without and disturbance like stirring for about 2 hours. Then 6 catalyst pieces (A1, A2, B1, B2, C1, C2) were taken out from each α -Al₂O₃ powder plate as shown below.

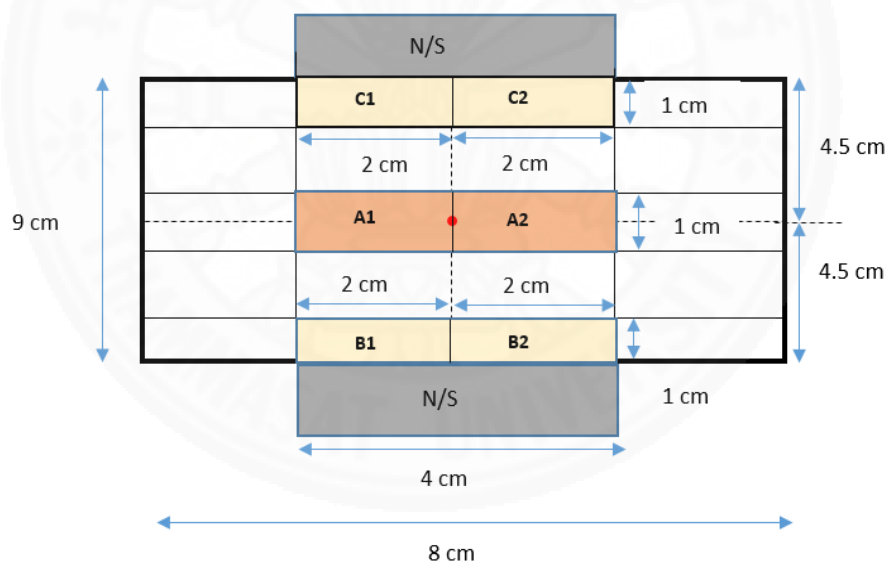


Figure 4.5 Geometrical dimension of α -Al₂O₃ powder plate.

Since the length of the magnet piece is 4cm, the catalyst pieces were taken of dimension (2 mm x 1 mm) to cover the strongest magnetic field areas. Then concentration of Cu²⁺ and Zn²⁺ ions within that specific area were determined through AAS. The following figures represent the concentration profile of each ion with reference to the center point (initial dropping).

4.2.1 Diffusion of Cu^{2+} ions on $\alpha\text{-Al}_2\text{O}_3$ support under magnetic inducement

Here the Cu^{2+} concentration embedded in each specific slot is displayed in ppm. In N-N and N-S magnetic pole arrangements the concentration of Cu^{2+} ions, in the catalysts obtained from very near to the 2 magnets in both ends for both magnetic pole arrangements are about twenty times higher than the Cu^{2+} concentration of respective catalysts in no magnetic field instance. Thus it is obvious that whatever the magnetic pole arrangement, magnetic inducement is capable to provide an external driving force for Cu^{2+} ions to be moved all over the support uniformly without being agglomerated in the center. Since there is no external force other than diffusion the concentration of Cu^{2+} ions far from the center in no magnetic inducement case is negligible.

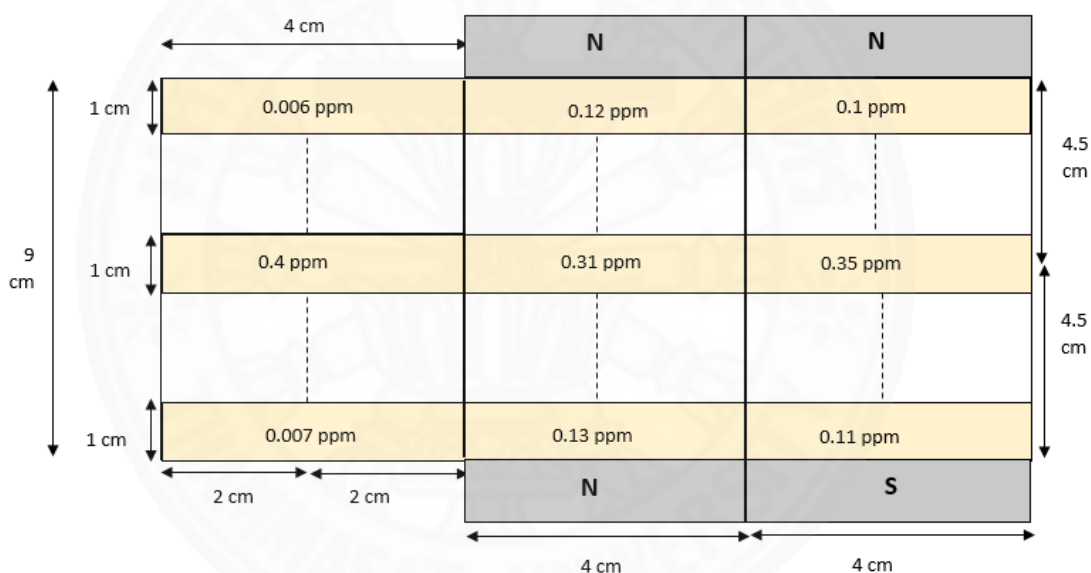


Figure 4.6 Concentration profile of diffusion of Cu^{2+} ions on $\alpha\text{-Al}_2\text{O}_3$ support.

4.2.2 Diffusion of Zn^{2+} ions on $\alpha\text{-Al}_2\text{O}_3$ support under magnetic inducement

Here also the Zn^{2+} concentration embedded in each specific slot is displayed in ppm. The concentrations of Zn^{2+} ions in catalysts very near to the magnets in both N-N and N-S instances are about eighteen times greater compared to the concentrations of Zn^{2+} ions in respective catalysts in no magnetic field instance. For Zn^{2+} also irrespective of the magnetic pole arrangement, magnetic inducement is capable to provide an external driving force for ions to be moved all over the support without being agglomerated in the center. However the concentrations of Zn^{2+} ions far from the center

point are apparently lower than the figures of Cu^{2+} ions in specific slots, implying that Cu^{2+} ions have a higher tendency in being distributed uniformly under magnetic inducement compared to Zn^{2+} ions. However, since there is no external force other than diffusion, the dispersion of Zn^{2+} ions in no magnetic field situation is almost negligible.

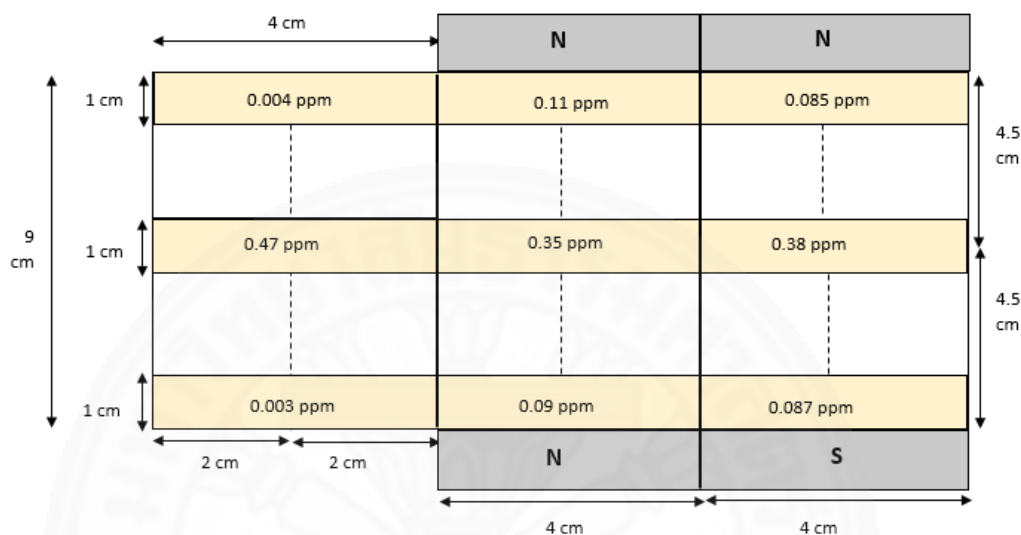


Figure 4.7 Concentration profile of diffusion of Zn^{2+} ions on $\alpha\text{-Al}_2\text{O}_3$ support.

4.2.3 Combined diffusion of Cu^{2+} and Zn^{2+} ions on $\alpha\text{-Al}_2\text{O}_3$ support under magnetic inducement

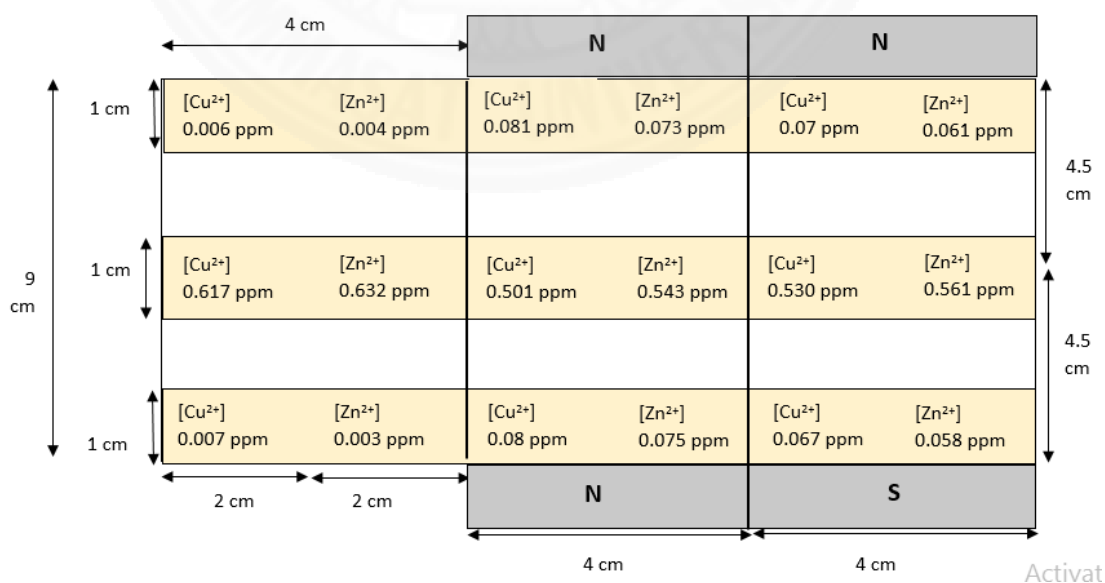


Figure 4.8 Concentration profile of diffusion of Cu^{2+} and Zn^{2+} ions on $\alpha\text{-Al}_2\text{O}_3$ support.

Figure 4.8 indicates how both Cu^{2+} and Zn^{2+} ions move parallelly on alpha alumina support. The concentrations of both Cu^{2+} and Zn^{2+} ions in catalysts near to the 2 magnets in both N-N and N-S instances are around 15 times and 13 times greater compared to the concentration of both Cu^{2+} and Zn^{2+} ions in respective catalysts of no magnetic field incident. Which imply that the combination of 2 ions has less capability of being homogeneously distributed throughout the support compared to their individual movements. Here also whatever the magnetic pole arrangement, the magnetic inducement is capable of providing an extra driving force for the motion of ions compared to the nonmagnetic field arrangement.

So depending on these basic results, it is obvious that magnetic inducement provides an external driving force for both Cu^{2+} and Zn^{2+} ions to be distributed all over any support without being agglomerated in specific locations likewise in nonmagnetic inducement incident. Thus it can be assumed that the application of magnetic inducement during Cu-Zn metal loading might provide a uniform dispersion of active metals over the support framework.

4.3 Effect of magnetic inducement on deposition and distribution of Cu and Zn active metals on support

Here 5wt% Cu-Zn active metals are loaded into the supports by applying a magnetic inducement during their sol-gel preparation. The effect of magnetic inducement during active metal loading was initially examined by preparing catalysts over in-house $\gamma\text{-Al}_2\text{O}_3$ support. Thus here are the preliminary catalysts prepared with different magnetic pole arrangements during their metal loading on $\gamma\text{-Al}_2\text{O}_3$ support and the later section describe the amount of hydrogen yield by each catalyst through MSR. The below three catalysts were tested for methanol steam reforming reaction at 200, 225, 250, 275 and 300 °C temperatures.

- 1) 5wt% Cu-Zn (no magnet)/In-house $\gamma\text{-Al}_2\text{O}_3$
- 2) 5wt% Cu-Zn (N-N)/ In-house $\gamma\text{-Al}_2\text{O}_3$
- 3) 5wt% Cu-Zn (N-S)/ In-house $\gamma\text{-Al}_2\text{O}_3$

4.3.1 Hydrogen production yield through MSR

Table 4.6 H₂ production rate over 5wt% Cu-Zn/ In-house γ -Al₂O₃ catalysts prepared with and without magnetic inducement.

Magnetic inducement and pole arrangement	H ₂ production rate (μ mol/min)				
	200 °C	225 °C	250 °C	275 °C	300 °C
No magnet	60 \pm 2	95 \pm 13	193 \pm 21	320 \pm 20	523 \pm 46
N-N	67 \pm 2	155 \pm 10	347 \pm 17	615 \pm 37	830 \pm 70
N-S	72 \pm 2	170 \pm 20	392 \pm 22	667 \pm 32	854 \pm 88

Table 4.4 shows H₂ production rates for Cu-Zn catalysts prepared via sol-gel method with and without magnetic inducement on In-house γ -Al₂O₃ support. There is a positive relationship between the amount of H₂ yield obtained and the reaction temperatures for every catalyst, but the effect of magnetic inducement on the catalytic activity is not that much noticeable at 200 °C and 300 °C. Here the catalyst prepared with N-S metal loading provides the highest hydrogen yield which is pretty much twice the yield given by catalyst made with no magnetic inducement within 225-275 °C temperature range.

For catalysts prepared over In-house γ -Al₂O₃ support, it is obvious that catalyst prepared with magnetic inducement provide significant higher hydrogen yield compared to the catalyst prepared with no magnetic field inducement. Thus the concentration profiles obtained through AAS justify that magnetic inducement provide an external driving force for the uniform distribution of active metals all over the support.

Thus by summarizing Table 4.1 and Table 4.4, it can be manifested that the same pole of magnetic inducement (N-N) applied during sol-gel preparation of CeO₂ doped Al₂O₃ support shows a significant improvement on the distribution of Ce on Al₂O₃ framework while during active metal loading, the opposite pole of magnetic inducement (N-S) enhances the active metal dispersion on the support.

Therefore, the sol-gel method together with the application of magnetic inducement during both support preparation and metal loading might be a potential technique for enhancing catalytic activity of Cu-Zn based catalyst for methanol steam reforming at low reaction temperature.

4.4 Effect of magnetic inducement during both support preparation and active metal loading on the support

The main goal of this section is to examine the combined effect of magnetic inducement during both support preparation and metal loading. Thus (N-S), (N-N) magnetic pole arrangements and no magnetic field were applied during the 5wt% Cu-Zn metal loading to following supports during their sol-gel preparation.

- 1) 5mol% CeO₂-doped Al₂O₃ (no magnet)
- 2) 5mol% CeO₂-doped Al₂O₃ (N-N)
- 3) 5mol% CeO₂-doped Al₂O₃ (N-S)

Thus three different catalyst types were prepared from each one of these supports depending on the magnetic pole arrangement applied during the metal loading. So here are the all nine catalysts we got finally with combined effect of magnetic inducement during support preparation and metal loading.

- A1) 5wt% Cu-Zn (no magnet)/5mol% CeO₂-doped Al₂O₃ (no magnet)
- A2) 5wt% Cu-Zn (N-N)/5mol% CeO₂-doped Al₂O₃ (no magnet)
- A3) 5wt% Cu-Zn (N-S)/5mol% CeO₂-doped Al₂O₃ (no magnet)

- B1) 5wt% Cu-Zn (no magnet)/5mol% CeO₂-doped Al₂O₃ (N-N)
- B2) 5wt% Cu-Zn (N-N)/5mol% CeO₂-doped Al₂O₃ (N-N)
- B3) 5wt% Cu-Zn (N-S)/5mol% CeO₂-doped Al₂O₃ (N-N)

- C1) 5wt% Cu-Zn (no magnet)/5mol% CeO₂-doped Al₂O₃ (N-S)
- C2) 5wt% Cu-Zn (N-N)/5mol% CeO₂-doped Al₂O₃ (N-S)
- C3) 5wt% Cu-Zn (N-S)/5mol% CeO₂-doped Al₂O₃ (N-S)

So same as earlier these nine different catalysts were tested for methanol steam reforming reaction at 200, 225, 250, 275 and 300 °C temperatures.

4.4.1 Hydrogen production yield through MSR

Table 4.7 H₂ production rate of 5wt% Cu-Zn catalyst prepared with and without magnetic inducement over 5mol% CeO₂-doped Al₂O₃ (no magnet) support.

Magnetic inducement and pole arrangement	H ₂ production rate (μmol/min)				
	200 °C	225 °C	250 °C	275 °C	300 °C
No magnet	150±30	371±43	619±61	950±50	1205±46
N-N	165±40	550±50	943±47	1565±81	1699±70
N-S	174±42	730±56	1306±62	1680±72	1782±81

Table 4.8 H₂ production rate of 5wt% Cu-Zn catalyst prepared with and without magnetic inducement over 5mol% CeO₂-doped Al₂O₃ (N-N) support.

Magnetic inducement and pole arrangement	H ₂ production rate (μmol/min)				
	200 °C	225 °C	250 °C	275 °C	300 °C
No magnet	175±50	754±60	1349±117	1800±137	2099±170
N-N	181±30	986±43	1865±53	2344±73	2400±58
N-S	195±22	1253±64	2146±82	2645±84	2796±76

Table 4.9 H₂ production rate of 5wt% Cu-Zn catalyst prepared with and without magnetic inducement over 5mol% CeO₂-doped Al₂O₃ (N-S) support.

Magnetic inducement and pole arrangement	H ₂ production rate (μmol/min)				
	200 °C	225 °C	250 °C	275 °C	300 °C
No magnet	167±42	530±40	916±42	1388±72	2002±88
N-N	177±31	890±10	1615±31	2240±64	2403±43
N-S	184±20	923±25	1728±32	2345±50	2474±73

These hydrogen yield tables prove that the combined effect of magnetic inducement during both support preparation and Cu-Zn metal loading provide a positive effect on activity of catalysts compared to the amount of hydrogen produced by the respective catalysts when magnetic field was applied separately. The 5wt% Cu-Zn (N-S)/5mol% CeO₂-doped Al₂O₃ (N-N) catalyst give the highest hydrogen yield within 225-275 °C proving our earlier fact that (N-N) magnetic pole arrangement during CeO₂-doped Al₂O₃ support preparation and (N-S) magnetic pole arrangement during Cu-Zn metal loading provide relatively perfect microstructure to have large number of well dispersed active sites.

Although there is no significant difference between the hydrogen yields given by following catalysts:

5wt% Cu-Zn (N-N)/5mol% CeO₂-doped Al₂O₃ (N-N)

5wt% Cu-Zn (N-S)/5mol% CeO₂-doped Al₂O₃ (N-N),

5wt% Cu-Zn (N-N)/5mol% CeO₂-doped Al₂O₃ (N-S)

5wt% Cu-Zn (N-S)/5mol% CeO₂-doped Al₂O₃ (N-S)

within the tested temperature range, it is clear that whatever the magnetic field applied during support preparation or metal loading, it provides a far more improved catalytic activity rather than the no magnetic field situation.



CHAPTER 5

CONCLUSION

The activity of Cu-Zn based catalysts for methanol steam reforming reaction can be improved by support modification and enhancing Cu-Zn active metal dispersion on the support. Thus in this study the catalytic activity of Cu-Zn catalyst for methanol steam reforming was enhanced by introducing magnetic inducement both during sol-gel preparations of the support and the catalyst.

Here support modification using partial doping of Ce into Al₂O₃ framework coupled with magnetic inducement to enhance the Ce distribution throughout the framework was studied for the cost effectiveness and the high surface area for an active Cu-Zn based catalyst. CeO₂-doped Al₂O₃ support can enhance the catalytic activity for hydrogen production and improve Cu-Zn dispersion over the CeO₂-doped Al₂O₃ support compared to γ -Al₂O₃. The magnetic inducement during sol-gel preparation of the support can affect Ce composition and the uniform dispersion of Ce in the Al₂O₃ framework. Cu-Zn/CeO₂-doped Al₂O₃ prepared with the same pole magnetic arrangement gives the highest H₂ production yield due to high composition of Ce and better uniform dispersion of Ce in Al₂O₃ framework. Thus once the partial doping of Ce into Al₂O₃ framework is coupled with magnetic inducement, it results a low cost approach to enhance the catalytic activity of Cu-Zn catalyst.

Further in order to experimentally study the diffusion pattern of Cu²⁺ and Zn²⁺ ions under the magnetic inducement in semi liquid state, series of Cu/ α -Al₂O₃, Zn/ α -Al₂O₃, and Cu-Zn/ α -Al₂O₃ catalysts were prepared with and without magnetic inducement. The concentration profiles obtained for each Cu²⁺ and Zn²⁺ ions with and without magnetic inducement, clearly described the effect of magnetic field towards the motion of ions. Thus through the AAS results it can be concluded that, magnetic inducement irrespective of the magnetic pole arrangement (both N-N and N-S) provide an external driving force for both Cu²⁺ and Zn²⁺ ions to be distributed all over any support without being agglomerated in specific locations likewise in nonmagnetic inducement incident.

In order to enhance Cu-Zn active metal dispersion on the support, magnetic inducement was applied during the sol-gel preparation of Cu-Zn catalyst. The effect of magnetic inducement during active metal loading was initially examined by preparing catalysts over in-house γ -Al₂O₃ support. Here catalysts prepared with magnetic inducement during metal loading provided significant higher hydrogen yield compared to the catalyst prepared with no magnetic field inducement. Thus in Cu-Zn active metal loading, the catalyst prepared with opposite pole magnetic inducement (N-S) gave the highest hydrogen yield within 225-275 °C and enhances the metal dispersion on the support.

The same pole magnetic arrangement applied during sol-gel preparation of CeO₂-doped Al₂O₃ support shows a significant improvement on the composition and distribution of Cu and Zn on the support. While, in Cu-Zn metal loading, the opposite pole of magnetic inducement (N-S) enhances the metal dispersion on the support. Thus irrespective of the magnetic pole arrangement the combined effect of magnetic inducement during both support preparation and Cu-Zn metal loading provide a positive effect on catalytic activity of Cu-Zn catalyst to yield higher hydrogen productions at lower reaction temperatures.

Support and catalyst preparation by sol-gel method with a magnetic inducement has a potential to be further investigated in depth study. Further experiments can be carried out to clearly decide out of two magnetic pole arrangements during both support and catalyst preparation which magnetic pole arrangement provide a significantly high hydrogen yield. And very precise chemisorption techniques should be carried out to clearly describe the combined dispersion of Cu-Zn active metals on γ -Al₂O₃ support and CeO₂-doped γ -Al₂O₃ support. Further changing in dimension and intensity of magnetic field can also be investigated since it can be one factor that could affect the final properties of the catalyst support.

REFERENCES

Journals/Periodicals

- Acar, C., & Dincer, I. (2014). Analysis and assessment of a continuous-type hybrid photoelectrochemical system for hydrogen production. *International Journal of Hydrogen Energy*, 39(28), 15362–15372.
<https://doi.org/10.1016/j.ijhydene.2014.07.146>
- Agarwal, V., Patel, S., & Pant, K. K. (2005). H₂ production by steam reforming of methanol over Cu / ZnO / Al₂O₃ catalysts : transient deactivation kinetics modeling, 279, 155–164. <https://doi.org/10.1016/j.apcata.2004.10.026>
- Agrell, J., Birgersson, H., Boutonnet, M., Melián-cabrera, I., Navarro, R. M., & Fierro, J. L. G. (2003). Production of hydrogen from methanol over Cu / ZnO catalysts promoted by ZrO₂ and Al₂O₃, 219, 389–403.
[https://doi.org/10.1016/S0021-9517\(03\)00221-5](https://doi.org/10.1016/S0021-9517(03)00221-5)
- Amiri, T. Y., & Moghaddas, J. (2016). Reaction parameters influence on the catalytic performance of copper-silica aerogel in the methanol steam reforming. *Journal of Fuel Chemistry and Technology*, 44(1), 84–90. [https://doi.org/10.1016/S1872-5813\(16\)30008-1](https://doi.org/10.1016/S1872-5813(16)30008-1)
- Azenha, C. S. R., Mateos-Pedrero, C., Queirós, S., Concepción, P., & Mendes, A. (2017). Innovative ZrO₂-supported CuPd catalysts for the selective production of hydrogen from methanol steam reforming. *Applied Catalysis B: Environmental*, 203, 400–407. <https://doi.org/10.1016/j.apcatb.2016.10.041>
- Baykara, S. Z. (2004). Experimental solar water thermolysis. *International Journal of Hydrogen Energy*, 29(14), 1459–1469.
<https://doi.org/10.1016/j.ijhydene.2004.02.011>
- Bedrane, S., Descorme, C., & Duprez, D. (2002). Towards the comprehension of oxygen storage processes on model three-way catalysts, 73, 233–238.
- Boaro, M., Vicario, M., De Leitenburg, C., Dolcetti, G., & Trovarelli, A. (2003). The use of temperature-programmed and dynamic/transient methods in catalysis: Characterization of ceria-based, model three-way catalysts. *Catalysis Today*, 77(4), 407–417. [https://doi.org/10.1016/S0920-5861\(02\)00383-8](https://doi.org/10.1016/S0920-5861(02)00383-8)
- Bouly, C., Chandes, K., Maret, D., & Bianchi, D. (1995). Characterization of surface

- and bulk oxygen species of three way catalysts by O₂ TPD and H₂ TPR. *Studies in Surface Science and Catalysis*, 96(C), 261–274.
[https://doi.org/10.1016/S0167-2991\(06\)81435-7](https://doi.org/10.1016/S0167-2991(06)81435-7)
- Cauqui, M. A. (1992). Application of the Sol – Gel Methods to Catalyst Preparation NON-CRYSTALLINE Application of the sol-gel methods to catalyst preparation, 3093(August 2018). [https://doi.org/10.1016/S0022-3093\(05\)80707-0](https://doi.org/10.1016/S0022-3093(05)80707-0)
- Chiu, Y. J., Chiu, H. C., Hsieh, R. H., Jang, J. H., & Syu, G. J. (2017). Experimental Study on the Reaction Conditions of a Methanol Steam Reforming Process. *Energy Procedia*, 105, 1622–1627. <https://doi.org/10.1016/j.egypro.2017.03.525>
- Cunningham, J., O'Brien, S., Sanz, J., Rojo, J. M., Soria, J. A., & Fierro, J. L. G. (1990). Exceptional susceptibility of ceria-supported rhodium catalyst to inhibitory SMSI effects including acetone hydrogenation. *Journal of Molecular Catalysis*, 57(3), 379–396. [https://doi.org/10.1016/0304-5102\(90\)85011-6](https://doi.org/10.1016/0304-5102(90)85011-6)
- Damyanova, S., Pawelec, B., & Arishtirova, K. (2008). Study of the surface and redox properties of ceria – zirconia oxides, 337, 86–96.
<https://doi.org/10.1016/j.apcata.2007.12.005>
- Damyanova, S., Perez, C. A., Schmal, M., & Bueno, J. M. C. (2002). Characterization of ceria-coated alumina carrier. *Applied Catalysis A: General*, 234(1–2), 271–282. [https://doi.org/10.1016/S0926-860X\(02\)00233-8](https://doi.org/10.1016/S0926-860X(02)00233-8)
- Danwittayakul, S., & Dutta, J. (2012). Zinc oxide nanorods based catalysts for hydrogen production by steam reforming of methanol, 7(0001), 1–9.
<https://doi.org/10.1016/j.ijhydene.2011.12.161>
- Danwittayakul, S., & Dutta, J. (2013). Two step copper impregnated zinc oxide microball synthesis for the reduction of activation energy of methanol steam reformation, 223, 304–308. <https://doi.org/10.1016/j.cej.2013.03.029>
- Das, D., & Veziroglu, T. N. (2008). Advances in biological hydrogen production processes. *International Journal of Hydrogen Energy*, 33(21), 6046–6057.
<https://doi.org/10.1016/j.ijhydene.2008.07.098>
- De Leitenburg, C., Trovarelli, A., & Kašpar, J. (1997). A temperature-programmed and transient kinetic study of CO₂ activation and methanation over CeO₂ supported noble metals. *Journal of Catalysis*, 166(1), 98–107.

<https://doi.org/10.1006/jcat.1997.1498>

- Doenitz, W., Schmidberger, R., Steinheil, E., & Streicher, R. (1980). Hydrogen production by high temperature electrolysis of water vapour. *International Journal of Hydrogen Energy*, 5(1), 55–63. [https://doi.org/10.1016/0360-3199\(80\)90114-7](https://doi.org/10.1016/0360-3199(80)90114-7)
- Duprez, D., Descorme, C., Birchem, T., & Rohart, E. (2001). Oxygen storage and mobility on model three-way catalysts, 1–8.
- Ebiad, M. A., Abd El-Hafiz, D. R., Elsalamony, R. A., & Mohamed, L. S. (2012). Ni supported high surface area CeO₂-ZrO₂ catalysts for hydrogen production from ethanol steam reforming. *RSC Advances*, 2(21), 8145–8156. <https://doi.org/10.1039/c2ra20258a>
- El Fallah, J., Boujana, S., Dexpert, H., Kiennemann, A., Majerus, J., Touret, O., ... Le Normand, F. (1994). Redox processes on pure ceria and on Rh/CeO₂ catalyst monitored by X-ray absorption (fast acquisition mode). *Journal of Physical Chemistry*, 98(21), 5522–5533. <https://doi.org/10.1021/j100072a020>
- Esposito, S. (2019). “ Traditional ” Sol-Gel Chemistry as a Powerful Tool for the Preparation of Supported Metal and Metal Oxide Catalysts, 1–25. <https://doi.org/10.3390/ma12040668>
- Fornasiero, P., Monte, R. Di, Kaspar, J., Meriani, S., Trovarelli, A., & Graziani, M. (1995). Rh-Loaded CeO₂-ZrO₂ Solid Solutions as Highly Efficient Oxygen Exchangers: Dependence of the Reduction Behavior and the Oxygen Storage Capacity on the Structural Properties. *Journal of Catalysis*.
- Franczak, A., Binnemans, K., & Fransaer, J. (2016). inhomogeneous magnetic fields †. *Physical Chemistry Chemical Physics*, 18, 27342–27350. <https://doi.org/10.1039/C6CP02575G>
- Fujiwara, M., Mitsuda, K., & Tanimoto, Y. (2006). Movement and diffusion of paramagnetic ions in a magnetic field. *Journal of Physical Chemistry B*, 110(28), 13965–13969. <https://doi.org/10.1021/jp061482p>
- Galvita, V., Messerle, V. E., & Ustimenko, A. B. (2007). Hydrogen production by coal plasma gasification for fuel cell technology. *International Journal of Hydrogen Energy*, 32(16), 3899–3906. <https://doi.org/10.1016/j.ijhydene.2007.05.039>

- Hak, S., Moon, J., Hun, J., Hong, J., Lee, J., Lee, H., ... Kim, H. (2016). Acta Materialia Panoscopic alloying of cobalt in CeO₂ e ZrO₂ solid solutions for superior oxygen-storage capacity. *Acta Materialia*, *113*, 206–212. <https://doi.org/10.1016/j.actamat.2016.04.060>
- Han, H. B., Guo, B., & Chai, F. (2012). Influence of magnetic field on aqueous nacl solutions: A foundational research on the desalination method based on the rotating electromagnetic effect. *Advanced Materials Research*, *591–593*, 2607–2611. <https://doi.org/10.4028/www.scientific.net/AMR.591-593.2607>
- He, Z., Yang, M., Wang, X., Zhao, Z., & Duan, A. (2012). Effect of the transition metal oxide supports on hydrogen production from bio-ethanol reforming. *Catalysis Today*, *194*(1), 2–8. <https://doi.org/10.1016/j.cattod.2012.05.004>
- Hickey, N., Fornasiero, P., Monte, R. Di, Kaspar, J., Graziani, M., & Dolcetti, G. (2001). A comparative study of oxygen storage capacity over Ce_{0.6}Zr_{0.4}O₂ mixed oxides investigated by temperature-programmed reduction and dynamic OSC measurements, *72*(1), 45–50.
- Holladay, J. D., Hu, J., King, D. L., & Wang, Y. (2009). An overview of hydrogen production technologies. *Catalysis Today*, *139*(4), 244–260. <https://doi.org/10.1016/j.cattod.2008.08.039>
- Hou, T., Zhang, S., Chen, Y., Wang, D., & Cai, W. (2015). Hydrogen production from ethanol reforming: Catalysts and reaction mechanism. *Renewable and Sustainable Energy Reviews*, *44*, 132–148. <https://doi.org/10.1016/j.rser.2014.12.023>
- Jakdetchai, O., Takayama, N., & Nakajima, T. (2005). Activity enhancement of CuZn-impregnated FSM-16 by modification with 1,3-butanediol for steam reforming of methanol. *Kinetics and Catalysis*, *46*(1), 56–64. <https://doi.org/10.1007/s10975-005-0009-8>
- Jeong, H., Kim, K. I., Kim, T. H., Ko, C. H., Park, H. C., & Song, I. K. (2006). Hydrogen production by steam reforming of methanol in a micro-channel reactor coated with Cu/ZnO/ZrO₂/Al₂O₃ catalyst. *Journal of Power Sources*, *159*(2), 1296–1299. <https://doi.org/10.1016/j.jpowsour.2005.11.095>
- Jin, T. Okuhara T., M. G. J. and W. J. M. (1987). Temperature-Programmed Desorption of CO and COP from Pt/CeO₂. for Lattice Oxygen in CO Oxidation.

- American Chemical Society*, 91(12), 3310–3315.
- Jin, H., Lu, Y., Liao, B., Guo, L., & Zhang, X. (2010). Hydrogen production by coal gasification in supercritical water with a fluidized bed reactor. *International Journal of Hydrogen Energy*, 35(13), 7151–7160.
<https://doi.org/10.1016/j.ijhydene.2010.01.099>
- Kolczyk, K., Kutyla, D., Wojnicki, M., Cristofolini, A., Kowalik, R., & Zabinski, P. (2016). SEparation of rare earth metals ions in a static magnetic field. *Magneto hydrodynamics*, 52(4), 541–547. <https://doi.org/10.22364/mhd.52.4.11>
- Kowalik, P., & Go, A. (2013). K INETIC CHARACTERISATION OF CATALYSTS FOR METHANOL SYNTHESIS, 34(4), 497–506. <https://doi.org/10.2478/cpe-2013-0040>
- Laosiripojana, N., & Assabumrungrat, S. (2008). Kinetic dependencies and reaction pathways in hydrocarbon and oxyhydrocarbon conversions catalyzed by ceria-based materials. *Applied Catalysis B: Environmental*, 82(1–2), 103–113.
<https://doi.org/10.1016/j.apcatb.2008.01.009>
- Latorre, N., Ubieto, T., Royo, C., & Romeo, E. (2006). Improvement of activity and stability of Ni – Mg – Al catalysts by Cu addition during hydrogen production by catalytic decomposition of methane, 116, 264–270.
<https://doi.org/10.1016/j.cattod.2006.05.085>
- Lei, H., Nie, R., Fei, J., & Hou, Z. (2012). Preparation of Cu / ZnO / Al₂O₃ catalysts in a solvent-free routine for CO hydrogenation *, 13(5), 395–406.
<https://doi.org/10.1631/jzus.A1100345>
- Li, P., Chen, X., Li, Y., & Schwank, J. W. (2018). A review on oxygen storage capacity of CeO₂-based materials : In fl uence factors , measurement techniques , and applications in reactions related to catalytic automotive emissions control. *Catalysis Today*, (May), 0–1. <https://doi.org/10.1016/j.cattod.2018.05.059>
- Li, P., Chen, X., Li, Y., & Schwank, J. W. (2019). A review on oxygen storage capacity of CeO₂-based materials: Influence factors, measurement techniques, and applications in reactions related to catalytic automotive emissions control. *Catalysis Today*, (May), 90–115. <https://doi.org/10.1016/j.cattod.2018.05.059>
- Li, Y., Guo, L., Zhang, X., Jin, H., & Lu, Y. (2010). Hydrogen production from coal gasification in supercritical water with a continuous flowing system.

- International Journal of Hydrogen Energy*, 35(7), 3036–3045.
<https://doi.org/10.1016/j.ijhydene.2009.07.023>
- Lorenz, H., Friedrich, M., Armbrüster, M., Klötzer, B., & Penner, S. (2013). ZnO is a CO₂-selective steam reforming catalyst, 297, 151–154.
<https://doi.org/10.1016/j.jcat.2012.10.003>
- Marquez, C., Rivera-torrente, M., Paalanen, P. P., Weckhuysen, B. M., Cirujano, F. G., Vos, D. De, & Baerdemaeker, T. De. (2017). Increasing the availability of active sites in Zn-Co double metal cyanides by dispersion onto a SiO₂ support. *Journal of Catalysis*, 354, 92–99. <https://doi.org/10.1016/j.jcat.2017.08.008>
- Martí, A., Ferná, M., Conesa, J. C., & Soria, J. (2000). Structural and Redox Properties of Ceria in Alumina-Supported Ceria Catalyst Supports, 4038–4046.
- Matsumura, Y., & Ishibe, H. (2009). Suppression of CO by-production in steam reforming of methanol by addition of zinc oxide to silica-supported copper catalyst. *Journal of Catalysis*, 268(2), 282–289.
<https://doi.org/10.1016/j.jcat.2009.09.026>
- McGuirk, G. M., Ledieu, J., Gaudry, É., De Weerd, M. C., & Fournée, V. (2014). Surface structures of In-Pd intermetallic compounds. I. Experimental study of in thin films on Pd(111) and alloy formation. *Journal of Chemical Physics*, 141(8).
<https://doi.org/10.1063/1.4892408>
- Mirjalili, F., Hasmaliza, M., & Abdullah, L. C. (2010). Size-controlled synthesis of nano α -alumina particles through the sol – gel method. *Ceramics International*, 36(4), 1253–1257. <https://doi.org/10.1016/j.ceramint.2010.01.009>
- Myronyuk, I. F., Mandzyuk, V. I., Sachko, V. M., & Gun'ko, V. M. (2016). Structural and Morphological Features of Disperse Alumina Synthesized Using Aluminum Nitrate Nonahydrate. *Nanoscale Research Letters*, 11(1).
<https://doi.org/10.1186/s11671-016-1366-0>
- Nath, K., & Das, D. (2004). Biohydrogen production as a potential energy resource - Present state-of-art. *Journal of Scientific and Industrial Research*, 63(9), 729–738.
- Ni, M., Leung, M. K. H., Sumathy, K., & Leung, D. Y. C. (2006). Potential of renewable hydrogen production for energy supply in Hong Kong. *International Journal of Hydrogen Energy*, 31(10), 1401–1412.

- <https://doi.org/10.1016/j.ijhydene.2005.11.005>
- Ogawa, K., & Koteka, A. Y. (1978). Copper Oxide-Zinc Oxide-Alumina Catalyst : of a Copper Oxide-Zinc Oxide-Alumina for Methanol Synthesis The Structure Catalyst, *205*, 191–205.
- Oguchi, H., Nishiguchi, T., Matsumoto, T., & Kanai, H. (2005). Steam reforming of methanol over Cu / CeO₂ / ZrO₂ catalysts, *281*, 69–73.
<https://doi.org/10.1016/j.apcata.2004.11.014>
- Papavasiliou, J., Avgouropoulos, G., & Ioannides, T. (2005). Steam reforming of methanol over copper – manganese spinel oxide catalysts, *6*, 497–501.
<https://doi.org/10.1016/j.catcom.2005.04.015>
- Papavasiliou, J., Avgouropoulos, G., & Ioannides, T. (2007). Effect of dopants on the performance of CuO – CeO₂ catalysts in methanol steam reforming, *69*, 226–234. <https://doi.org/10.1016/j.apcatb.2006.07.007>
- Pintado, J. M. (2004). Characterisation of three-way automotive aftertreatment catalysts and related model systems, *28*(April).
- Rakoczy, J., Nizioł, J., Wieczorek-Ciurowa, K., & Dulian, P. (2013). Catalytic characteristics of a copper-alumina nanocomposite formed by the mechanochemical route. *Reaction Kinetics, Mechanisms and Catalysis*, *108*(1), 81–89. <https://doi.org/10.1007/s11144-012-0503-8>
- Rameshan, C., Stadlmayr, W., Penner, S., Lorenz, H., Memmel, N., Hävecker, M., ... Klötzer, B. (2012). Angewandte Hydrogen Production by Methanol Steam Reforming on Copper Boosted by Zinc-Assisted Water Activation **, 3002–3006. <https://doi.org/10.1002/anie.201106591>
- Rameshan, C., Stadlmayr, W., Penner, S., Lorenz, H., Memmel, N., Hävecker, M., ... Klötzer, B. (2012). Hydrogen production by methanol steam reforming on copper boosted by zinc-assisted water activation. *Angewandte Chemie - International Edition*, *51*(12), 3002–3006.
<https://doi.org/10.1002/anie.201106591>
- Reungsang, A., Zhong, N., & Yang, Y. (2018). *Hydrogen from Photo Fermentation*. Springer Singapore. <https://doi.org/10.1007/978-981-10-7677-0>
- Riedo, E., Brune, H., Heiz, U., Ferrari, A. M., Giordano, L., Pacchioni, G., ... Uni, V. (2001). Identification of Defect Sites on MgO (100) Thin Films by Decoration

- with Pd Atoms and Studying CO Adsorption Properties, (100), 6172–6178.
- Rikken, R. S. M., Nolte, R. J. M., Maan, J. C., Van Hest, J. C. M., Wilson, D. A., & Christianen, P. C. M. (2014). Manipulation of micro- and nanostructure motion with magnetic fields. *Soft Matter*, *10*(9), 1295–1308.
<https://doi.org/10.1039/c3sm52294f>
- Rodrigues, I. R., Lukina, L., Dehaeck, S., Colinet, P., Binnemans, K., & Fransaeer, J. (2017). Magnetomigration of Rare-Earth Ions Triggered by Concentration Gradients. *Journal of Physical Chemistry Letters*, *8*(21), 5301–5305.
<https://doi.org/10.1021/acs.jpcllett.7b02226>
- SAKAMOTO, Y., KIZAKI, K., MOTOHIRO, T., YOKOTA, Y., SOBUKAWA, H., UENISHI, M., ... SUGIURA, M. (2002). New Method of Measuring the Amount of Oxygen Storage/Release on Millisecond Time Scale on Planar Catalyst. *Journal of Catalysis*, *211*(1), 157–164.
<https://doi.org/10.1006/jcat.2002.3715>
- Sari, A., & Sabziani, J. (2017). Modeling and 3D-simulation of hydrogen production via methanol steam reforming in copper-coated channels of a mini reformer. *Journal of Power Sources*, *352*, 64–76.
<https://doi.org/10.1016/j.jpowsour.2017.03.120>
- Shi, Z. M., Liu, Y., Yang, W. Y., Liang, K. M., Pan, F., & Gu, S. R. (2002). Evaluation of cordierite – ceria composite ceramics with oxygen storage capacity, *22*, 1251–1256.
- Shishido, T., Yamamoto, Y., Morioka, H., Takaki, K., & Takehira, K. (2004). Active Cu/ZnO and Cu/ZnO/Al₂O₃ catalysts prepared by homogeneous precipitation method in steam reforming of methanol. *Applied Catalysis A: General*, *263*(2), 249–253. <https://doi.org/10.1016/j.apcata.2003.12.018>
- Sun, J. T., Metcalfe, I. S., & Sahibzada, M. (1999). Deactivation of Cu / ZnO / Al₂O₃ Methanol Synthesis Catalyst by Sintering, 3868–3872.
- TADA, T. (2011). *Introduction to Elementary Particles 3. Radioisotopes* (Vol. 60).
<https://doi.org/10.3769/radioisotopes.60.527>
- Trovarelli, A. (1996). Catalytic properties of ceria and CeO₂-Containing materials. *Catalysis Reviews - Science and Engineering*, *38*(4), 439–520.
<https://doi.org/10.1080/01614949608006464>

- Trueba, M., & Trasatti, S. P. (2005). γ -Alumina as a Support for Catalysts : A Review of Fundamental Aspects, 3393–3403.
<https://doi.org/10.1002/ejic.200500348>
- Tsai, M., Wang, J., Shen, C., & Yeh, C. (2011). Promotion of a copper – zinc catalyst with rare earth for the steam reforming of methanol at low temperatures, 279, 241–245. <https://doi.org/10.1016/j.jcat.2010.12.018>
- Udani, P. P. C., Gunawardana, P. V. D. S., Lee, H. C., & Kim, D. H. (2009). Steam reforming and oxidative steam reforming of methanol over CuO – CeO₂ catalysts, 34, 7648–7655. <https://doi.org/10.1016/j.ijhydene.2009.07.035>
- Vacharapong, P., Arayawate, S., Henpraserttae, S., Katanyutanon, S., Charojrochkul, S., Lawtrakul, L., & Toochinda, P. (2019). Effect of Magnetic Inducement in Preparation of Ni/Ce-doped Al₂O₃ for Ammonia Decomposition. *ChemistrySelect*, 4(40), 11913–11919. <https://doi.org/10.1002/slct.201902663>
- Volovych, I. (2014). Sol-gel processes in catalysis : catalyst synthesis , application , recycling and combination to tandem reactions in microemulsions.
- Wang, J. B., Tsai, D., & Huang, T. (2002). Synergistic Catalysis of Carbon Monoxide Oxidation over Copper Oxide Supported on Samaria-Doped Ceria, 380, 370–380. <https://doi.org/10.1006/jcat.2002.3580>
- Wang, L., Liu, Q., Chen, M., Liu, Y., Cao, Y., He, H., & Fan, K. (2007). Structural Evolution and Catalytic Properties of Nanostructured Cu / ZrO₂ Catalysts Prepared by Oxalate Gel-Coprecipitation Technique, 16549–16557.
<https://doi.org/10.1021/jp075930k>
- Wang, L., Liu, Y., Chen, M., Cao, Y., He, H., Wu, G., ... Fan, K. (2007). Production of hydrogen by steam reforming of methanol over Cu / ZnO catalysts prepared via a practical soft reactive grinding route based on dry oxalate-precursor synthesis, 246, 193–204. <https://doi.org/10.1016/j.jcat.2006.12.006>
- Yang, H., & Liao, P. (2007). Preparation and activity of Cu / ZnO-CNTs nano-catalyst on steam reforming of methanol, 317, 226–233.
<https://doi.org/10.1016/j.apcata.2006.10.018>
- Yao, Y. U. (1984). Ceria in Automotive Exhaust Catalysts, 265, 254–265.
- Zhang, L., Pan, L. W., Ni, C. J., Sun, T. J., Wang, S. D., Hu, Y. K., ... Zhao, S. S. (2013). Effects of precipitation aging time on the performance of

CuO/ZnO/CeO₂-ZrO₂ for methanol steam reforming. *Ranliao Huaxue Xuebao/Journal of Fuel Chemistry and Technology*, 41(7), 883–888.

[https://doi.org/10.1016/s1872-5813\(13\)60038-9](https://doi.org/10.1016/s1872-5813(13)60038-9)

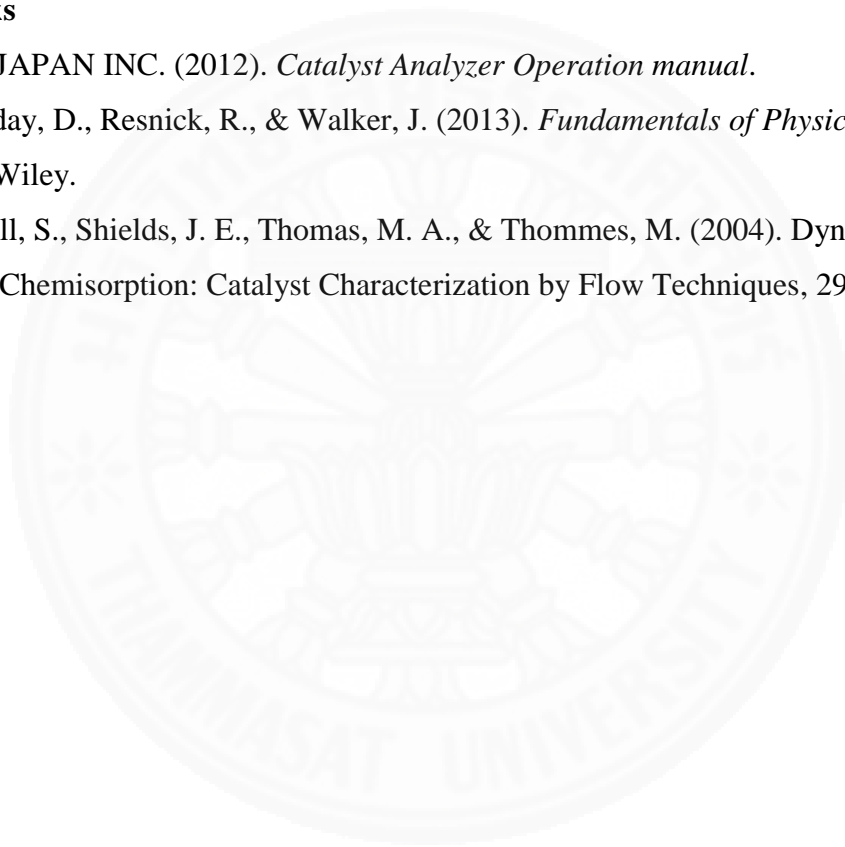
Zhu, G. P., Hejiazan, M., Huang, X., & Nguyen, N. T. (2014). Magnetophoresis of diamagnetic microparticles in a weak magnetic field. *Lab on a Chip*, 14(24), 4609–4615. <https://doi.org/10.1039/c4lc00885e>

Books

BEL JAPAN INC. (2012). *Catalyst Analyzer Operation manual*.

Halliday, D., Resnick, R., & Walker, J. (2013). *Fundamentals of Physics Extended*. Wiley.

Lowell, S., Shields, J. E., Thomas, M. A., & Thommes, M. (2004). Dynamic Chemisorption: Catalyst Characterization by Flow Techniques, 297–310.





APPENDIX A

SUPPORT AND CATALYST PREPARATION

A.1 CeO₂-doped Al₂O₃ support preparation

Here, 15 grams of 5mol% CeO₂-doped in Al₂O₃ was prepared by sol-gel method in different magnetic pole arrangements for methanol steam reforming reaction. CeO₂-doped Al₂O₃ supports were prepared from the nitrate precursor, Ce from Ce(NO₃)₃.6H₂O and Al from Al(NO₃)₃.9H₂O. The amount of chemicals used in the preparation are shown in Table A.2 and Table A.3, respectively with sample calculations.

Table A.1 Molecular weight of related metals or compounds in support preparation.

Element/Compound	Mw (g/mol)
Ce	140.12
Al	26.98
Ce(NO ₃) ₃ .6H ₂ O	434.22
Al(NO ₃) ₃ .9H ₂ O	375.13

Table A.2 Calculated amount of metals used in support preparation.

Metal	Mole fraction in support	Weight (g)	Weight in 15 g of support (g)
Ce	0.05	7.01	3.22
Al	0.95	25.63	11.78
Total	1.00	32.64	15.00

Sample calculation of 5mol% CeO₂-doped Al₂O₃ for methanol steam reforming:

$$\begin{aligned} \text{Ce}_{\text{prepared support}} \text{ (g)} &= \frac{0.05 \frac{\text{mol Ce}}{\text{mol Ttotal}} \times 140.12 \frac{\text{g Ce}}{\text{mol Ce}}}{28.11 \text{ gtotal mol fraction weight}} \times 15 \text{ g support} \\ &= 3.74 \text{ g} \end{aligned}$$

$$\begin{aligned} \text{Al}_{\text{prepared support}} \text{ (g)} &= \frac{0.95 \frac{\text{mol Al}}{\text{mol Ttotal}} \times 26.98 \frac{\text{g Al}}{\text{mol Al}}}{28.11 \text{ gtotal mol fraction weight}} \times 15 \text{ g support} \\ &= 13.67 \text{ g} \end{aligned}$$

Table A.3 Calculated amount of compounds used in support preparation.

Compound	Weight in compound form required (g)	Total volume of individual 0.5M salt solution (mL)
Ce(NO ₃) ₃ .6H ₂ O	11.59	53.38
Al(NO ₃) ₃ .9H ₂ O	190.07	1013.34

Sample calculation of 5mol% CeO₂-doped Al₂O₃ for methanol steam reforming:

$$\text{Ce(NO}_3)_3 \cdot 6\text{H}_2\text{O weight (g)} = 3.74_{\text{g}_{\text{Ce}}} \times \frac{434.22_{\text{g}_{\text{Ce(NO}_3)_3 \cdot 6\text{H}_2\text{O}}}}{140.12_{\text{g}_{\text{Ce}}}}$$

$$= 11.59 \text{ g}$$

$$\text{Total volume of 0.5 M Ce salt solution (mL)} = \frac{3.74_{\text{g}_{\text{Ce}}}}{140.12_{\frac{\text{g}_{\text{Ce}}}{\text{mol}_{\text{Ce}}}}} \times \frac{1000_{\text{mL}_{\text{salt solution}}}}{0.5_{\text{mol}_{\text{Ce}}}}$$

$$= 53.38 \text{ mL}$$

$$\text{Al(NO}_3)_3 \cdot 9\text{H}_2\text{O weight (g)} = 13.67_{\text{g}_{\text{Al}}} \times \frac{375.13_{\text{g}_{\text{Al(NO}_3)_3 \cdot 9\text{H}_2\text{O}}}}{26.98_{\text{g}_{\text{Al}}}}$$

$$= 190.07 \text{ g}$$

$$\text{Total volume of 0.5 M Al salt solution (mL)} = \frac{13.67_{\text{g}_{\text{Al}}}}{26.98_{\frac{\text{g}_{\text{Al}}}{\text{mol}_{\text{Al}}}}} \times \frac{1000_{\text{mL}_{\text{salt solution}}}}{0.5_{\text{mol}_{\text{Al}}}}$$

$$= 1013.34 \text{ mL}$$

A.2 Catalyst preparation

Cu-Zn/5mol% CeO₂-doped Al₂O₃ catalysts were also prepared with and without magnetic inducement. Here 5 g of Cu-Zn catalysts with 5wt% Cu-Zn over supports were prepared by sol-gel method with and without magnetic inducement. The amount of chemicals used in the preparation are shown in Table A.5 with sample calculations.

Table A.4 Molecular weight of related metals or compounds in catalyst preparation.

Element/Compound	Mw (g/mol)
Cu	63.55
Zn	65.39
Cu(NO ₃) ₂ .3H ₂ O	241.59
Zn(NO ₃) ₂ .6H ₂ O	297.48
C ₆ H ₈ O ₇ (citric acid)	192.12

Table A.5 Calculated amount of compounds used in catalyst preparation.

Amount of Cu in 5 g of catalyst (g)	0.125
Amount of Cu(NO ₃) ₂ .3H ₂ O (g)	0.47
Amount of Zn in 5 g of catalyst (g)	0.125
Amount of Zn(NO ₃) ₂ .6H ₂ O	0.57
Amount of C ₆ H ₈ O ₇ (citric acid) (g)	0.81
Amount of DI water (mL)	3.12
Amount of support (g)	4.75

Sample calculation of 5wt% Cu-Zn on catalysts:

5 g of catalyst with 5wt% Cu-Zn = 0.125 g of Cu + 0.125 g of Zn + 4.75 g of support

$$\begin{aligned} \text{Amount of Cu(NO}_3)_2 \cdot 3\text{H}_2\text{O (g)} &= 0.125_{\text{gCu}} \times \frac{241.59_{\text{gCu(NO}_3)_2 \cdot 3\text{H}_2\text{O}}}{63.55_{\text{gCu}}} \\ &= 0.47 \text{ g} \end{aligned}$$

$$\begin{aligned} \text{Amount of Zn(NO}_3)_2 \cdot 6\text{H}_2\text{O (g)} &= 0.125_{\text{gZn}} \times \frac{297.48_{\text{gZn(NO}_3)_2 \cdot 6\text{H}_2\text{O}}}{65.39_{\text{gZn}}} \\ &= 0.57 \text{ g} \end{aligned}$$

$$\begin{aligned} \text{Amount of DI water (mL)} &= (\text{Amount of Cu(NO}_3)_2 \cdot 3\text{H}_2\text{O (g)} + \text{Amount of Zn(NO}_3)_2 \cdot 6\text{H}_2\text{O (g)}) \times 3 \\ &= (0.47 \text{ g} + 0.57 \text{ g}) \times 3 \\ &= 3.12 \text{ mL} \end{aligned}$$

$$\begin{aligned} \text{Amount of citric acid (g)} &= (\text{Amount of Cu(NO}_3)_2 \cdot 3\text{H}_2\text{O (g)} + \text{Amount of Zn(NO}_3)_2 \cdot 6\text{H}_2\text{O (g)}) \times 0.78 \\ &= (0.47 \text{ g} + 0.57 \text{ g}) \times 0.78 \\ &= 0.81 \text{ g} \end{aligned}$$

APPENDIX B

CHEMISORPTION TECHNIQUE

In this study, as mentioned in chapter 2, temperature programmed reduction technique using H_2 as the probe is carried out. The description of the chemisorption operation is described as follows.

B.1 Temperature-programmed reduction (TPR)

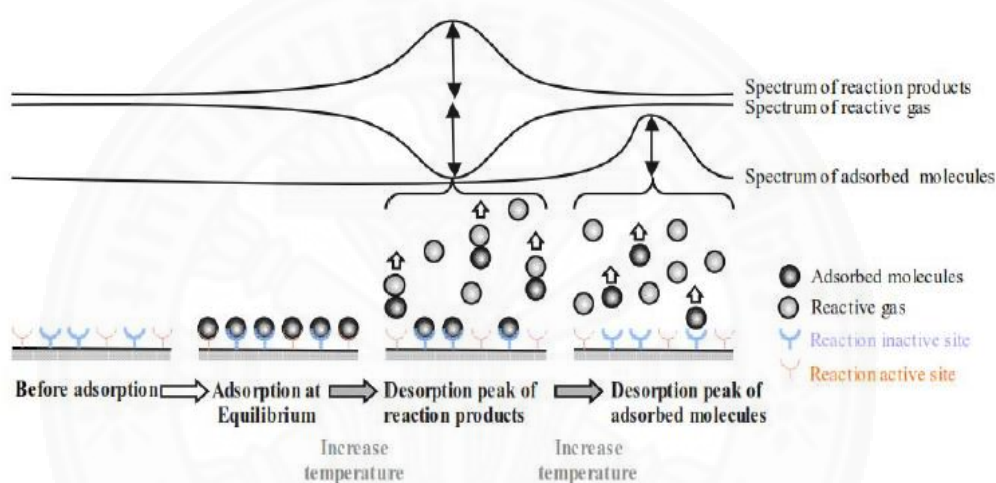


Figure B.1 Diagram for temperature-programmed reduction (TPR) and temperature-programmed oxidation (TPO) explanation (BEL JAPAN INC., 2012).

This is a dynamic chemisorption, operated in temperature-programmed mode. Temperature-programmed reduction (TPR) is used to study the reduction behavior of the oxide-form active sites by using reducing gas. The mixture comprises of 5% H_2 with 95% Ar is used as a reducing probe gas, and flowed onto the material surface. The sample temperature, which is normally lower than the reduction temperature, is increased with constant heating rate. The reduction occurs when hydrogen gas is consumed in the reduction process and detected by Thermal Conductivity Detector (TCD). The water, a common product from reduction reaction, is needed to be trapped out before reaching TCD, otherwise the detector will function improperly and damaged (in long run). When reduction is complete, there is no hydrogen gas consumption, the TCD signal is back to the baseline. Reduction peaks are from the different types of

oxides on the catalyst surface which requires the different amount of energy needed to undergo reduction which is related to the weak or strong metal-support interaction. The peak height is directly related to the reduction reaction rate, and the peak area is related to the amount of reduced species at particular temperature.



BIOGRAPHY

Name Mrs. Dilpium Samarasinghe
Date of Birth October 17, 1991
Education 2017: Honours Degree of Bachelor of the Science of
Engineering
Faculty of Engineering
University of Moratuwa
Sri Lanka

Publications

Samarasinghe, D., Gadavanij, I., Soontornpakornkit, N., Muangkumbutr, N., Katanyutanon, S., Arayawate, S, & Toochinda, P. (2019). Effects of magnetic inducement on Cu-Zn/Al₂O₃ catalyst for methanol steam reforming. In *The Pure and Applied Chemistry International Conference 2019 (PACCON2019)* (CS75-79).